THE ASTRONOMICAL JOURNAL VOLUME 107, NUMBER 6 JUNE 1994

DYNAMICS OF BINARY GALAXIES. II. CLOSE PAIRS

JAYARAM N. CHENGALUR
NAIC and Cornell University, Ithaca, New York 14853

E. E. SALPETER
CRSR and Cornell University, Ithaca, New York 14853

YERVANT TERZIAN
NAIC and Cornell University, Ithaca, New York 14853

Received 1993 December 7; revised 1994 January 31

ABSTRACT

As part of a comprehensive study of binary galaxies, broadband optical CCD images and high resolution H I maps are presented for six close pairs of spiral galaxies. A previous paper [Chengalur, *et al.*, ApJ, 419, 30 (1993)] presented the results of a study of binary galaxies with wide separations. The current sample of close pairs was chosen from the CfA redshift catalog using selection criteria that were objective and completely independent of any previously known morphological peculiarities. Nonetheless, all the galaxies show some sign of interaction, implying that the selection criteria were sufficiently well tailored to choose physically associated pairs. All the galaxies show kinematical disturbances and have asymmetric rotation curves. Tidal tails and bridges are clearly detected for some, and two pairs have a large common H I envelope. This common H I envelope also shows a large scale radial velocity gradient and gives the impression of being in rotation about a single kinematical axis. There is relatively good agreement between the optical and H I images, with similar tidal features being seen in both. The H I features, however, extend to a much larger galactocentric radius than the corresponding optical features. In at least one case, however, the stellar disk appears relatively normal, while the H I disk appears disturbed even towards the center of the galaxy. The systematic velocity difference for the galaxy pairs has been measured quite accurately either from the integrated H I spectral profile, or from a global fit to the galaxy velocity fields. The median velocity difference for the six galaxy pairs is very small, $\sim$20 km s^{-1}. Detailed analysis of the data will be presented in a separate paper.

1. INTRODUCTION

The observed flat rotation curves of spiral galaxies convincingly establishes the existence of an extended dark matter component. In general, the edge of the dark matter distribution cannot be determined from an analysis of the rotation curve, and the total galaxy mass is instead usually estimated from the dynamics of binary galaxies and small groups of galaxies. Such studies of binary galaxies include those by Page (1958), Karachentsev (1972), Turner (1976), Peterson (1979), White (1981), van Moorsel (1982), White *et al.* Davis (1983), Schneider *et al.* (1986), Schweizer (1987), Soares (1990), Sharp (1990), Charlton & Salpeter (1991), Schneider & Salpeter (1992) and Chengalur *et al.* (1993, Paper I).

Good velocity accuracy is essential in such studies of binary galaxies, and for spiral galaxies this is easiest obtained by H I observations. Galaxy pairs with good H I measurements are, however, biased against very close pairs because of the confusion caused by the poor resolution of single dish radio telescopes. In addition, close galaxy pairs are likely to be disturbed, making it difficult to determine the systemic velocity from the global profile. Both these problems can be solved by using a radio interferometer which has sufficient angular and velocity resolution to be able to map out the emission from the two galaxies in the pair. Such observations not only determine the systemic velocity of the galaxies but also trace out the kinematical and morphological disturbances of the gas disks. The exact form of the tidal disturbance depends on the mass distribution in the galaxy pair and their previous orbital history, and is hence interesting.

An interferometric study of galaxy pairs was done by van Moorsel (1982), who presented Westerbok observations of H I emission from 14 pairs of galaxies. The selection criteria for van Moorsel's sample were tailored in order to avoid pairs which are likely to have tidal disturbances. However it is precisely these close, interacting, but pre-merger galaxy pairs that we are interested in for this study. Our sample hence does not overlap with van Moorsel's. Apart from numerous studies of individual, noteworthy interacting pairs, van Moorsel's work appears to be the only systematic interferometric study of the dynamics of galaxy pairs.

The sample selection criteria for this study are objective and completely independent of any previously known peculiarities in the morphology of the galaxy pairs. Another significant departure of this work from earlier studies is that the galaxy pairs are restricted to lie in regions of low local galaxy density. Six close pairs thus chosen were observed using

 0004-6256/94/107(6)/1984/22/$0.90

both the Very Large Array[1] (VLA) and the Hale 200 in telescope at Palomar.[2]

As discussed above, observations of close, interacting, but pre-merger galaxy pairs are useful not only in order to fill the gap at small separations in the samples observed at single dish radio telescopes, but also to determine orbital parameters such as the eccentricity. Information on the extended H I tidal features and velocity fields is crucial for determining the mass distribution in the pair, because, as emphasized by Sharp (1990), masses derived from binary galaxy studies depend critically on the orbital eccentricity, which is very poorly constrained by the single dish data. In addition, most recent theoretical work on binary galaxy interactions have concentrated on pairs that start in high eccentricity, low energy orbits, get sharply braked by dynamic friction, and rapidly merge. Detailed studies of the morphology and kinematics of an objectively chosen sample of close galaxy pairs provide an observational foil to such simulations. These and other theoretical issues and more sophisticated data analysis will be presented in a later paper (Chengalur *et al.* 1994); the current paper is restricted to a presentation of the data and other derived observational quantities which do not depend on the details specific theoretical models.

The sample selection criteria are discussed in Sec. 2, and the observations and data reduction procedure in Sec. 3. Broadband CCD images and H I maps are presented in Sec. 4, and, in Sec. 5, quantitative parameters measured from the CCD and H I images are tabulated.

2. Sample Selection Criteria

A sample of close binary galaxies was chosen from the CfA redshift catalog, (Huchra *et al.* 1983). The selection criteria were as follows.

(1) The galaxies had to lie in a region of low local galaxy density. The density was determined from a count of neighbors in a truncated cone with radius 4.5 Mpc and depth 335 km s^{-1} (H_0=75 km s^{-1} Mpc^{-1}). This count was corrected for the CfA selection function and for edge effects to give the final density [see Paper I and Chengalur (1994) for details]. This effectively discriminates against pairs in clusters and groups.

(2) The heliocentric redshift of both galaxies in the pair had to be between 1400 and 5000 km s^{-1}.

(3) The projected separation of each pair had to be less than 75 kpc and the velocity difference had to be less than 200 km s^{-1}

(4) Each galaxy in the pair had to be of type Sa or later (using morphological types from the CfA catalog).

(5) The total integrated H I flux for the pair (from previous single dish measurements) had to be greater than 10.0 Jy km s^{-1}.

This left us with seven galaxy pairs, which are listed in Table 1. The columns are as follows: Col. (1) UGC name of the galaxy. Cols. (2) and (3) 1950 epoch right ascension and declination of the galaxy. Col. (4) heliocentric velocity of the galaxy (from Haynes & Giovanelli 1992). Col. (5) the integrated H I flux for the galaxy in mJy km s^{-1} (from Haynes & Giovanelli 1992). Col. (6) the width of the H I profile of the galaxy, in km s^{-1} (from Haynes & Giovanelli 1992). Col. (7) the Holmberg diameters for the galaxy in arcminutes (from the RC3, de Vaucouleurs *et al.* 1992). Col. (8) B_T^0 magnitude for the galaxy (from the RC3), except for UGC 9903-4, for which the UGC magnitude is listed since the RC3 does not give magnitudes for these galaxies. Col. (9) the angular separation of the galaxy pair, in arcminutes.

TABLE 1. Sample of close pairs chosen from the CfA catalog.

Name (UGC)	RA (1950)	Dec (1950)	V_{Helio} (km s^{-1})	HI Flux (Jy km s^{-1})	HI Width (km s^{-1})	Dia (arcmin)	B (mag)	$\Delta\theta$ (arcmin)
U 4905	09 14 09.5	42 12 37	1733	8.50	324	2.6 × 0.8	12.53	
U 4909	09 14 18.1	42 12 15	1882	9.60	356	1.9 × 0.5	13.72	1.6
U 4995	09 20 39.8	49 25 08	2732	10.51	317	1.7 × 0.6	13.32	
U 4997	09 20 53.6	49 27 48	2638			1.0 × 0.5	13.50	3.5
U 5271	09 47 23.9	13 03 00	1440	43.20	247	2.9 × 1.7	12.17	
U 5275	09 47 45.8	13 00 06	1417	19.49	263	1.8 × 0.5	12.77	6.1
U 9724	15 05 11.1	19 47 27	4772			1.2 × 0.6	13.42	
U 9728	15 05 19.0	19 46 25	4764	9.31	476	2.7 × 0.6	12.36	2.1
U 9903	15 32 13.2	15 21 40	1983	4.27	143	1.6 × 1.2	(13.3)	
U 9904	15 32 15.7	15 22 10	1955	7.20	275	1.0 × 0.5	(13.7)	0.8
U12442	23 12 01.9	04 13 33	2648	37.70	305	1.9 × 0.5	12.69	
U12447	23 12 10.3	04 15 43	2678	35.41	469	3.1 × 1.0	11.59	3.0
U12737	23 38 55.7	03 27 43	2891	11.59	220	1.4 × 0.9	13.82	
U12738	23 39 0.0	03 26 50	2907	18.91	245	1.7 × 0.6	13.31	1.4

Despite the fact that the selection process does not involve explicit consideration of any morphological peculiarities, five out of these seven pairs are listed (in the UGC) as showing signs of interaction, implying that the selection criteria are sufficiently well tailored to choose physically associated galaxy pairs. The UGC notes for these pairs are given below.

UGC 4905−9: "arc of barely resolved knots curves into nucleus of larger galaxy (Arp),"

UGC 4995−9: "narrow tail leads away from nucleus (Arp),"

UGC 5271−5: "asymmetric bar, several ill defined filaments,"

UGC 9903−4: "spiral galaxy with large high surface brightness companion on arms (Arp)," "broad peculiar arm to companion, then absorption, faint extension from companion (Arp),"

UGC 12737−8: "disrupted, badly dented Sc."

3. OBSERVATIONS AND DATA REDUCTION

Due to constraints on observing time at the VLA, the pair with the longest estimated integration time in Table 1 (UGC 4905-9) was not observed. The remaining six pairs were observed in the C array of the VLA and also in the *R* band using the Hale 200 in telescope at Palomar. Four of these six were also observed in the *V* band (UGC 9724−8 and UGC 9903-4 were not observed in the *V* band). In addition to the C configuration observations, two pairs (UGC 4995−7 and

[1]The National Radio Astronomy Observatory is operated by the Associated University Inc., under contract with the National Science Foundation.

[2]Observations at the Palomar Observatory were made as part of a continuing collaborative agreement between the California Institute of Technology and Cornell University.

TABLE 2. Summary of the VLA and Palomar observations.

Name (UGC)	Array (C/D)	Obs Time (min)	Chan Sep (km s^{-1})	θ_{synth} (arcsec)	S_{rms} (mJy/Bm)	Filter (R/V)	Exp. Time (sec)
U 4995-7	C	288	21	28	0.4	R	600
	D	161	42	80	0.5	V	600
U 5271-5	C	197	21	31	0.6	R	300
						V	300
U 9724-8	C	188	21	24	0.4	R	600
U 9903-4	C	199	21	24	0.5	R	300
U12737-8	C	245	21	29	0.4	R	300
						V	300
U12442-7	C	127	21	33	0.6	R	300
	D	28	42	38	4.8	V	300

UGC 12442-7), were also observed in the VLA D array. The observations are summarized in Table 2. The columns are as follows: Col. (1) the UGC name of the galaxy pair. Col. (2) the VLA configuration in which the observation was made. Col. (3) the total on source integration time, in minutes. Col. (4) the channel separation, in km s^{-1}. Col. (5) the major axis size of the "natural weight" synthesized beam, in arcseconds. (Note: for the D array observation of U12442-7, the beam size is for the "uniform weight," case (see Sec. *3.2*). Col. (6) the rms noise level, in mJy/Bm in the final maps. Col. (7) the band in which the Palomar observation was made. Col. (8) the total exposure time in seconds.

3.1 VLA Observations

The VLA C array observations were carried out in two sessions, the first on 1992 of May 17 and the second on 1992 of May 22. The D array observations were conducted during "test time" for the array, and show broad low level (~2 mJy) striations probably due to solar emission. This, along with the short durations of the observations limits the dynamic range of the final maps.

The setup of the backend for the C array observations was the relatively new 4ABCD mode, in which each field is simultaneously observed in two partially overlapping spectral bands. Each band had a width of 3.125 MHz, and 32 spectral channels. The band centers were chosen to give an overlap of 12 channels between the two bands, resulting in a total velocity coverage of ~900 km s^{-1}, and a channel spacing of ~20 km s^{-1} (after online HANNING smoothing). The observations were split into 40 min scans with a phase calibrator being observed for 5 min between scans. The scans of different galaxies were interleaved as much as possible, to maximize UV coverage. VLA primary flux calibrators (3C48,3C286) were observed for 10 min at the start and end of each run.

The D array observations (which were conducted almost a year earlier than the C array observations) used the 2AC mode with a bandwidth of 6.25 MHz, and a total of 32 channels with a channel spacing of ~40 km s^{-1} (after online HANNING smoothing). The galaxies were observed for shorter scans of 20 min each, with observations of a phase calibrator between scans. A VLA primary flux calibrator was observed at the start and end of each run.

3.2 VLA Data Reduction

The VLA data reduction was done using tasks in the standard NRAO data reduction package AIPS. Bad visibilities were flagged and absolute gain and bandpass calibration was applied. Each field of view was mapped using the utility HORUS. First a large scale, low resolution map was prepared and inspected for bright continuum sources. Detected sources were CLEANed and the clean components used to remove these sources by subtraction in the UV plane (task UVSUB). After this maps of the individual channels were made and stacked in a three dimensional "DIRTY" cube, with spatial dimensions along the first two axes and radial velocity along the third axis. A continuum image determined from the average of the line free channels was then subtracted from all the planes in the "DIRTY" cube. For the C array observations, only one edge of each band was free of line emission, while for the D array observations, both ends of the band were free of line emission. In the latter case the continuum image was generated by the task IMLIN. The D configuration maps show low level striations due to solar interference, the continuum image was allowed to have a linear dependence on frequency to remove some of this structure without simultaneously removing genuine line emission. The next step in the data processing was to interpolate over the gaps in the UV coverage, using the CLEAN algorithm as coded in the utility APCLN. The final maps were stacked into a three dimensional CLEAN cube.

For the C configuration observations, all of the above data reduction steps were applied independently to each of the two spectral bands observed for each field of view. The final step was to join together the CLEAN cubes from each band, to give a total velocity coverage ~900 km s^{-1}, and to correct for the sensitivity pattern of the primary beam of the individual 25 m telescopes of the VLA.

For each field of view, maps were made using both "uniform" and "natural" weighting. Uniform weighting reduces the emphasis on small baselines, and consequently results in a smaller synthesised beam size, but also poorer sensitivity to extended structure as compared to natural weighting. Uniform weighted maps and natural weighted maps hence carry somewhat complementary information. However, since natural weighting emphasizes the shorter baselines, natural weighted data is also more susceptible to corruption by solar radiation. For the short D array observation on UGC 12442−7, this effect is large enough to make the natural weighted data difficult to interpret.

3.3 Palomar Observations

The Palomar observations were obtained on the night of 1992 December 3 using the four shooter. The primary aim of the observing run was to image a large region of the sky surrounding the pair UGC 12442−7, in order to identify the optical counter part to a cluster of radio sources in that region (see Sec. *4.6* for details). The images of the galaxy pairs were taken just before and after systematically mapping the region around UGC 12442−7.

The night was not photometric, and in addition there was substantial moon light for part of the night. Consequently the

images are not suitable for absolute photometry, but can be used to determine the morphology of the galaxies. The seeing averaged slightly better than 1.2 arcsec. Each of the galaxy pairs was observed in the Gunn *R* filter, four pairs were also observed in the Johnson *V* filter. The typical exposure time for each filter was 5 min. In the afternoon before the observing run dome-flats were taken for each camera and each filter, and dark exposures were taken for each camera. Just before the observing run, a series of exposures of the twilight sky were taken to use as sky-flats. Exposures of a standard star were taken using all four cameras in quick succession in order to determine the relative gains. The field of view of each camera of the four shooter is slightly larger than 4′ by 4′, in general therefore both galaxies in a pair do not fit onto a single CCD chip. In some cases where it was difficult to ensure that both galaxies in a pair do not fall near a chip boundary, two exposures slightly offset from one another were made.

3.4 Palomar Data Reduction

The Palomar data was reduced using the standard NOAO data reduction package IRAF. All frames were corrected for a constant bias level using the overscan line. The next step was to produce a suitable flatfield. The twilight-flats showed large scale striations which are not present in the exposures taken once the sky had become dark. The observations themselves consisted of many exposures on regions of the sky with no extended objects. There were approximately 30 such exposures for each camera in the *R* filter and approximately 20 exposures per camera in the *V* filter. These exposures were median filtered, to produce the flatfield. Bad pixels, or columns of pixels were fixed by simple linear interpolation over neighboring pixels, and images of a standard star were used to solve for the telescope pointing. However, a comparison of the positions of the galaxies determined in this manner from the accurate published positions showed that the telescope pointing drifted considerably. In cases where the discrepancy was large, the galaxy positions were set to those from the published literature.

A background image was then fit and removed from each frame. The background used was either a constant, or (for those few exposures taken when there was still a significant amount of moonlight), of second order. After this, the chips were scaled to a common level using the relative gains of the four cameras and the resulting images were mosaiced together, either by simply copying (with appropriate offsets) the pixels of each image into the final mosaic, or, (in the case where more that one exposure of a given pair had been taken), using the MOSAIC software kindly provided by S. T. Megeath (see Chengalur 1994; Megeath 1993) for details.

4. RESULTS OF THE OBSERVATIONS OF CLOSE PAIRS

4.1 Introduction

In this section the CCD images and the H I integrated emission maps and velocity fields for the six galaxy pairs (UGC 4995−7, UGC 5271−5, UGC 9724−8, UGC 9903−4, UGC 12442−7, and UGC 12737−8) are presented.

In general it is expected that the H I maps and the CCD images will show similar features, however, for interacting galaxies, misalignments of the optical and kinematical axes are not uncommon. Since the H I maps have relatively poor resolution, the CCD images are also useful to check for bars, spiral arms, and other fine scale features in the galaxies. As mentioned in Sec. 1, the exact form of the morphological or kinematical disturbance is important not only to establish that the galaxies are definitely associated, but also in order to determine the previous history of the binary orbits. Many of the details noted here will be referred to in the later analysis paper (Chengalur *et al.* 1994).

The integrated H I emission maps and the H I velocity fields were computed using the AIPS task MOMNT which computes the first three moments (i.e., 0, 1, and 2) of the velocity profile over the entire emission region. However, the maps differ from a simple integration along the velocity axis, because a given pixel is included in the computation only if its flux after smoothing in both position and velocity space is larger than a given threshold. The advantage of this scheme is that it preferentially discriminates against high spatial frequency noise. Note that the moment method tends to produce smooth velocity fields even if there is gas at two separate velocities along a given line of sight. Beam smearing also affects velocity fields derived using MOMNT, causing a small but systematic decrease in the radial velocity along the major axis, particularly in the inner regions where the radial velocity gradient is large. Another method for deriving the velocity field is to decompose the velocity profile along a given line of sight into multiple Gaussian components, determine which peak is relevant, and use the radial velocity of that peak to produce the velocity fields (see, e.g. Begeman 1987). This method is less susceptible than the moment method to the effects of beam smearing (Begeman 1987). In our case, however, the MOMNT method suffices, because the galaxies are in general disturbed and a sophisticated analysis of the rotation curve to determine the various mass components is therefore not warranted; the small systematic bias of the MOMNT method is not very crucial. Further, even when there is H I at multiple velocities along a given line of sight, the galaxy disk is so disturbed that it is usually impossible to determine uniquely which particular velocity is the one that is applicable.

The integrated H I spectrum for all the galaxies is presented. The H I velocity field is shown both in the form of isovelocity contours, superposed on greyscales and as position velocity diagrams along the major axes of the galaxies. The direction of rotation along the major axis is usually very easily established from these figures. Detecting gas rotating around the optical center of a galaxy is important for two reasons: (1) it confirms that the gas is, in fact, associated with that particular galaxy and (2) it establishes the spin sense of the galaxy. If the galaxy has spiral arms, then by assuming that the arms are trailing, the ambiguity in the spatial direction of the spin vector can be resolved, and the spatial orientation of the galaxy disk can be determined. Spiral galaxies are widely regarded as having trailing spiral arms, note however that simulations of strong tidal interactions in a retrograde encounter show the formation of a lead-

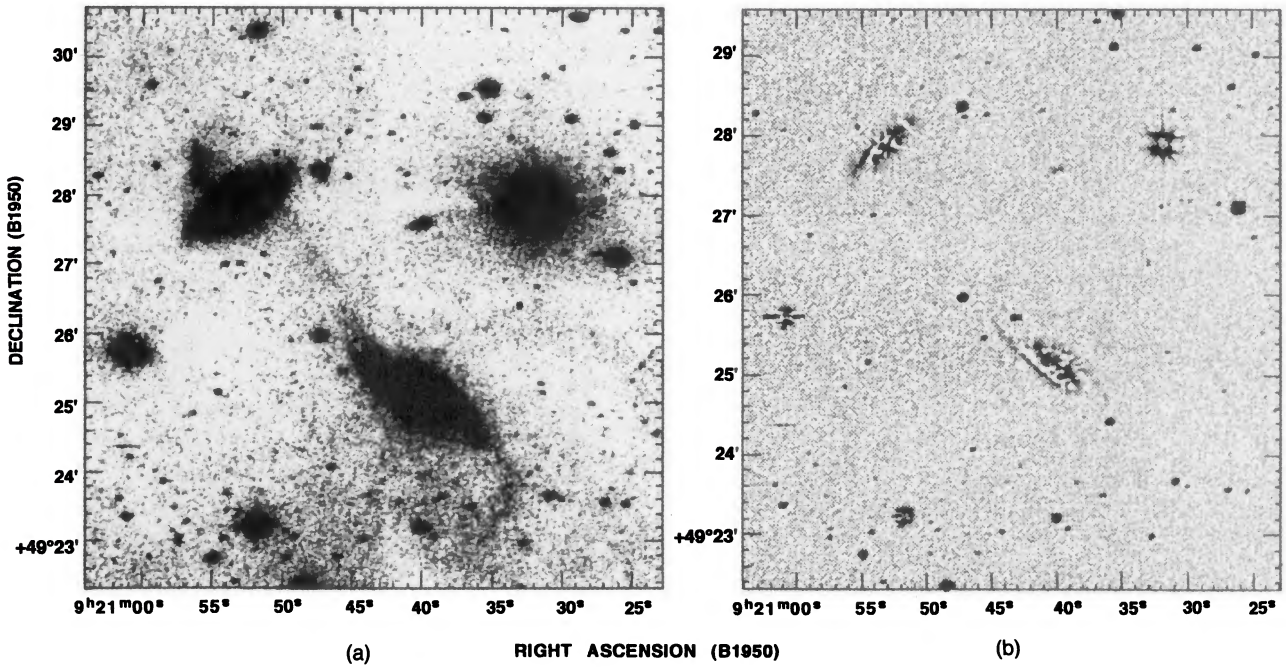

FIG. 1. (a) *V* band image for UGC 4995−7. UGC 4995 is at the lower right and UGC 4997 is at the upper left. (b) Unsharp filtered *V* band image for UGC 4995−7.

ing (but always single armed) spiral pattern (Thomasson *et al.* 1989).

4.2 UGC 4995−7

The *V* band image for UGC 4995−7, [Fig. 1(a)], shows a long tail extending to the south-west of UGC 4995 and a faint bridge connecting the two galaxies. Further, a bright chain of knots and accompanying diffuse emission can be seen along a line pointing to the north-east from the nucleus of UGC 4997 [this feature is also seen in the Arp atlas (Arp 1966)]. The *R* band image is similar, and is not shown. The unsharp filtered *V* band image [Fig. 1(b)], shows UGC 4995 to be a two armed barred spiral, with a knot of bright emission at the south-west end of the bar. UGC 4997 is also a two armed barred spiral [see Fig. 1(b)], with a bright central nuclear region.

The C configuration H I images are shown in Fig. 2(a) for the natural weight map and Fig. 2(b) for the uniform weight map. In both the maps, the optical centers are shown by large crosses while the tips of the major and minor axes are marked by smaller crosses. The position angle used is that measured from our CCD images, and the axes lengths are set to the Holmberg diameter, as listed in the RC3 (de Vaucouleurs *et al.* 1991). The beam size is 29″ for the natural weight C configuration maps and 12″ for C configuration uniform weight maps.

The natural weighted H I map shows a bridge connecting the two galaxies, as well as a long extended tail to the UGC 4995, in good concordance with the *V* band image Fig. 1(a). Both these features are also clearly seen in the D configuration map. For UGC 4995 the higher resolution map [Fig. 2(b)] brings out the lumpy distribution of H I in the galaxy, with the highest column density region at the south-west end of the galaxy, at the same location as the bright knot seen in the broad band optical images.

The H I distribution near UGC 4997 is quite disturbed, the apparent major axis of the H I distribution is perpendicular to the optical major axis of the galaxy. However, a more careful inspection shows that there is a barely discernible elongation of the H I distribution along the optical major axis of the galaxy, and a large amount of H I emission above the galactic plane (i.e., in the region near the north-eastern knots seen in the optical images). Finally, there is emission just to the south-west of the galaxy disk that is seen in both C configuration maps (as well as the D configuration map).

Isovelocity contours for the velocity field as derived from the natural weight C configuration H I maps is shown in Fig. 3. The velocity fields derived from the uniform weight C and D configuration data are similar and are not shown. As before, large crosses mark the optical galaxy centers, and the smaller crosses mark the tips of the optical major and minor axes.

For UGC 4995, there are deviations from simple circular rotation, including a slight misalignment between the optical and kinematical major axis, and nonorthogonality of the kinematical major and minor axes, which is perhaps related to the central bar [see for example, numerical simulations by Miller & Smith (1979)]. The position velocity diagram along the optical major axis of UGC 4995 (using the higher resolution, uniform weight data) is shown in Fig. 4. The gas with the falling radial velocity (corresponding to the closing velocity contours of Fig. 3) can be seen clearly at a relative position of −10 arcsec and −200 km s^{-1}. This is also the region where the long H I bridge connecting the two galaxies begins. Note that in this region there is also gas at two dif-

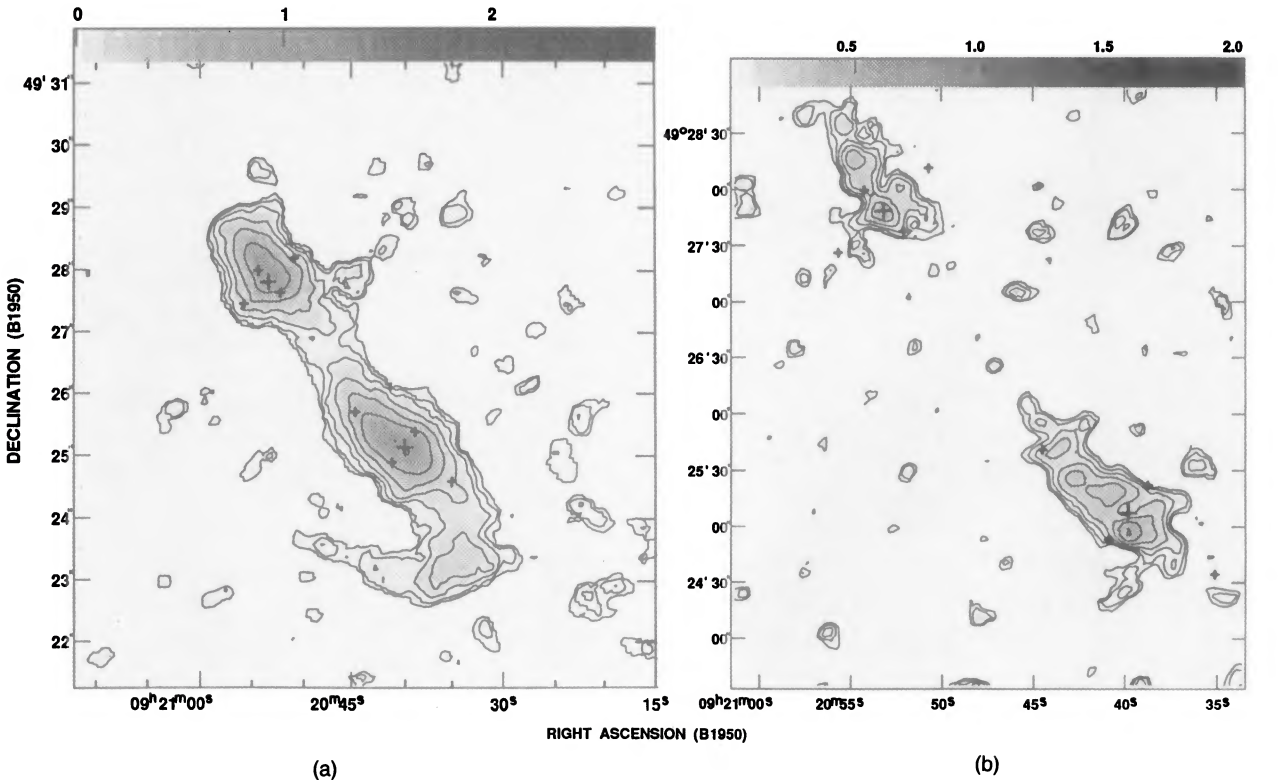

FIG. 2. (a) Contours of constant integrated H I flux for UGC 4995−7, made from the C configuration, natural weight data. The synthesized beam size is 29″. The contour levels are at 0.03, 0.04, 0.06, 0.09, 0.14, 0.20, 0.29, 0.42, 0.60, 0.88, and 1.28 Jy Bm^{-1} km s^{-1} (~4.0×10^{19} to ~1.7×10^{21} atoms cm^{-2}). The greyscales range from 0 to 3 Jy Bm^{-1} km s^{-1}. The large crosses mark the optical centers while the small crosses mark the tips of the major and minor axes. (b) Contours of constant integrated H I flux for UGC 4995−7, made from the C configuration, uniform weight data. The synthesized beam size is 12″. These contour levels are at 0.06, 0.09, 0.13, 0.19, 0.28, 0.41, and 0.6 Jy Bm^{-1} km s^{-1} (~4.6×10^{20} to ~4.6×10^{21} atoms cm^{-2}). The greyscales range from 0.03 to 2 Jy Bm^{-1} km s^{-1}. The large crosses mark the optical galaxy center, and the smaller crosses mark the tips of the optical major and minor axes.

ferent velocities along the line of sight, which is also often the case for severely warped disks.

In the case of UGC 4997, the velocity field is complex, and the apparent kinematical minor axis is badly misaligned with the optical minor axis. To clarify the H I distribution near UGC 4997, consider Fig. 5. This is a set of position velocity diagrams (using the higher resolution uniform weight data), with the horizontal axis measuring distance in arcseconds along the major axis of UGC 4997. The origin of the velocity axis is at a heliocentric velocity of 2900 km s^{-1}. The four panels are for cuts parallel to the major axis, and run from just above the major axis to just below the major axis of the galaxy. Panel (c) is the cut along the major axis, while the panels (a) and (b) include primarily H I from the region of strong H I emission north of the galaxy.

From the figure it is clear that at the lower velocities (relative velocities below −200 km s^{-1}), there is H I emission both from the UGC 4997 and from the bridge connecting the galaxies. In fact, one can see that at a relative position of 60″ there are at least two distinct peaks of the H I emission; clearly interpretation of the moment velocity field is difficult. Similarly, the integrated spectrum is not particularly illuminating, and is not shown. However, the direction of rotation can be relatively unambiguously determined, the north-western half of the galaxy has the higher heliocentric velocity.

Figure 6 is a position velocity plot along the H I bridge, including both galaxies. Radial velocity along the bridge varies smoothly from the radial velocity of UGC 4995 to that of UGC 4997. In the figure, UGC 4997 is the long vertical structure near a relative position ~−100 arcsec and UGC 4997 is the weaker vertical structure at ~100 arcsec and downwards of ~−300 km s^{-1}. The integrated H I spectrum for UGC 4995 is shown in Fig. 7.

4.3 UGC 5271−5

The *R* band CCD image for UGC 5271−5 is shown in Fig. 8, the *V* band image is very similar and is not shown. Faint emission can be seen extending from UGC 5275 towards UGC 5271.

UGC 5271 is a barred spiral galaxy, with a wealth of fine scale structure. There are several, very patchy spiral arms, and the unsharp filtered *V* image (not included), shows that in addition to the knots on the spiral arms, there is a set of knots approximately symmetrically placed on either side of the central bar.

UGC 5275 is a highly inclined galaxy, and much of its internal structure is obscured. There are several barely discernible hot spots at the edge of the galaxy image, and in addition, the central plane appears to be warped (unsharp filtered image, not included). The galaxy has a central bar and two knots of emission which are symmetrically offset from the bar. Thus, UGC 5275 too has a wealth of fine structure, and it appears likely, that given a favorable viewing angle, it would appear much like UGC 5271.

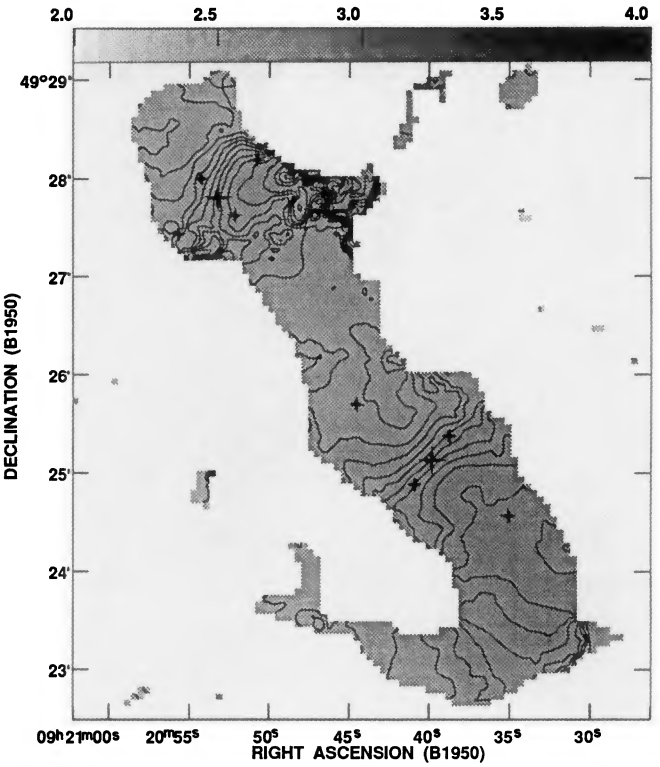

FIG. 3. H I velocity field for UGC 4995−7 (natural weight). There are 30 uniformly spaced contours between 2420 and 3000 km s^{-1} (i.e., 20 km s^{-1} apart). The greyscale range is from 2000 to 4000 km s^{-1}. The large crosses mark the optical galaxy center, and the smaller crosses mark the tips of the optical major and minor axes.

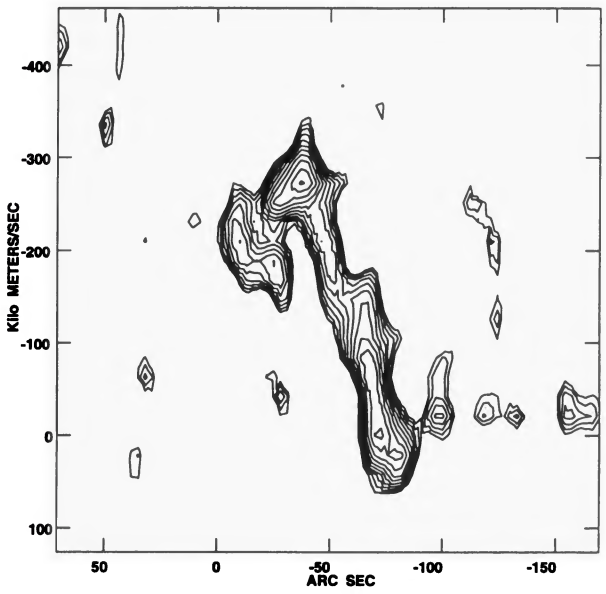

FIG. 4. Contours of constant emission intensity for a cut along the optical major axis of UGC 4995 [see Fig. 1(a)]. The horizontal axis measures distance parallel to the major axis in arcseconds (the galaxy center is at −62″, north-east is to the left), velocity (relative to 2900 km s^{-1}) is along the vertical axis. The contours are at 0.90, 1.04, 1.20, 1.39, 1.60, 1.85, 2.14, 2.47, 2.85, 3.29, and 3.80 mJy Bm^{-1}. From the high resolution uniform weight data.

A third galaxy can be seen in the CCD images, due south of UGC 5271 (i.e., at coordinates $09^h47^m25^s+13°58.8'$). This is NGC 3019, a 15th magnitude (CGCG magnitudes) galaxy, with a morphological type of spiral (UGC notes), and no published redshift. UGC 5275 (the fainter of the two galaxies in the pair of interest) has a magnitude of 13.7 on the same CGCG scale.

The H I integrated emission map (natural weight C configuration), is shown in Fig. 9. The uniform weight map is similar and is not shown. The galaxies do not show much signs of tidal disturbance, except for a slight distortion of UGC 5275 on the side closest to UGC 5271. The optical centers as well as the tips of the major and minor axes (with lengths corresponding to the Holmberg diameter) are shown with large and small crosses as before. Note that NGC 3019 is not detected, suggesting its radial velocity lies outside our observed 900 km s^{-1} wide band, or that it is very gas poor.

The uniform weight velocity map is shown in Fig. 10. Position velocity maps along the optical major axis of the two galaxies (derived from the uniform weight data) are shown in Fig. 11. Panel (a) (UGC 5271) is a relatively canonical looking position velocity diagram but with a slight asymmetry. The rotation curve flattens out at the high velocity end, but at the low velocity end the radial velocity appears to fall at the very tip of the major axis. UGC 5275 has a strongly asymmetric position velocity diagram. The velocity gradient decreases, but does not flatten out at the high velocity end, while at the low velocity end (i.e. in the region corresponding to the broad extension towards UGC 5271), where it appears to become flat, the profiles are broad with a non-Gaussian shape.

The integrated H I spectra are shown in Figs. 12 and 13. The systemic velocity, and the total velocity width as derived from these profiles agree extremely well with the Arecibo measurements (note that this pair was the only one with angular separation large enough to be resolved at Arecibo). For both UGC 5271 and UGC 5275, the kinematical minor axis is relatively well aligned with the optical minor axis. However for UGC 5275 there is a very strong asymmetry between the approaching and receding sides of the galaxy, in addition to a sharp twisting of the kinematical major axis in the outer region of the disk. This strong twisting of the kinematical major axis is usually indicative of a warped H I distribution. For UGC 5271 the isovelocity contours have a sharp kink near the major axis, this is probably related to central bar. Figure 10 also shows that the lowest velocity contour for UGC 5271 is closed.

4.4 UGC 9724−8

The *R* band images for UGC 9724−8 are shown in Fig. 14, there is no *V* band image for this galaxy pair. Both galaxies have central bulges and more diffuse halos, with the position angle of bulge being slightly misaligned with that of the halo. The galaxy images are fairly smooth, with no sign of much internal structure, or tidal disturbances (however, note that the image does not go very deep, the size of the visible galaxy disk is smaller than the Holmberg diameter listed in the RC3, in contrast to the previous images). In the

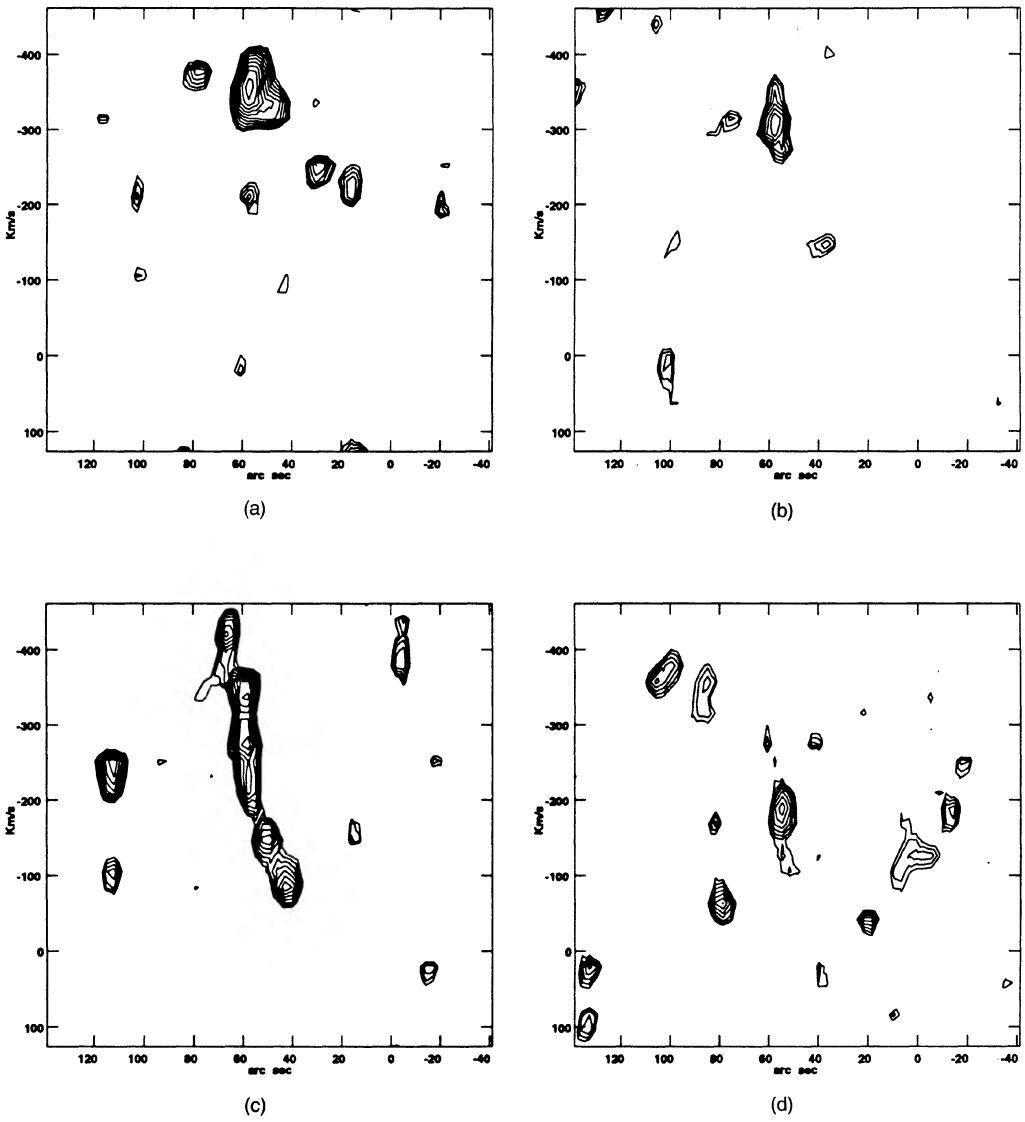

FIG. 5. Contours of constant H I intensity for a cut parallel to the major axis of UGC 4997 [see Fig. 1(a)]. Cut (a) is 18 arcsec above the galaxy center cut (b) is 9 arcsec above the galaxy center, cut (c) is through the galaxy center, and cut (d) is 9 arcsec below the galaxy center. Distance along the major axis (in arcseconds) is along the horizontal axis, (the galaxy center is at 57″, south-east is to the left), and velocity relative to 2900 km s^{-1} is along the vertical axis. The contours are at 0.90, 0.99, 1.09, 1.20, 1.32, 1.45, 1.60, 1.76, 1.94, 2.14, and 2.35 mJy Bm^{-1}. From the high resolution uniform weight data.

unsharp filtered *R* band image (not shown), a faint bar in UGC 9728 can be seen, while for UGC 9724, only the central bulge remains after unsharp filtering.

The C configuration integrated H I intensity maps are shown in Fig. 15(a) (natural weight) and Fig. 15(b) (uniform weight). Both galaxies have a hole in the H I distribution in the center of the galaxy (for UGC 9724, this is more clearly seen in the uniform weight map). The centers of the H I distributions of each galaxy appear shifted towards the other galaxy as compared to the optical positions. This shift may not be significant, however, since the optical positions are known to only about 10″ accuracy, and the separation between the galaxy centers as measured from the *R* band image is consistent with the separation as measured from the H I maps. In the natural weight map one can also see a bridge of material in between the two galaxies. Even in the higher resolution maps the bridge can be seen, however it is seen only at the point where the separation of the two galaxies is minimum (~20″); it is possible that the "bridge" is merely an effect of beam smearing. Examination of the individual channel maps however shows that not all the emission can be explained as beam smearing; there appears to be a genuine bridge of material joining the two galaxies.

The velocity field is shown in Fig. 16 (natural weight). The position velocity maps (using the natural weight data) are shown in Fig. 17. Panel (a) is a cut along the major axis of UGC 9724, and panel (b) is a cut along the major axis of UGC 9728. The opposite sense of rotation of the two galaxies can be clearly seen in these figures. The bridge connecting the two galaxies is at a relative position of ~25″, note

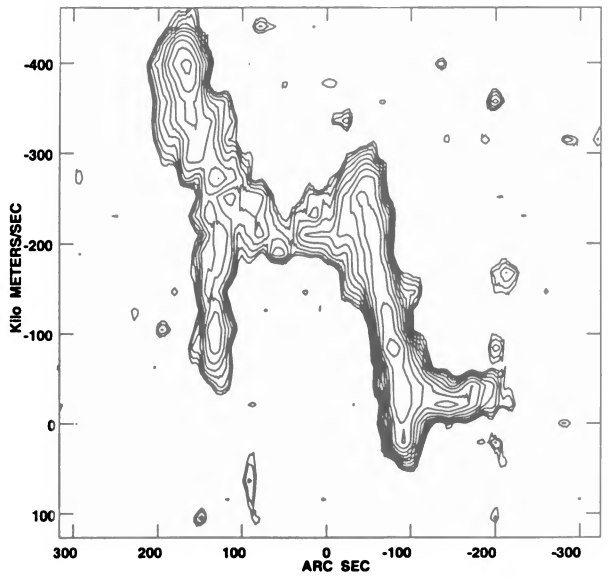

FIG. 6. Contours of constant H I intensity for a cut along the H I bridge connecting UGC 4995 and UGC 4997. The horizontal axis measures distance parallel to the bridge in arc seconds, velocity (relative to 2900 km s^{-1}) is along the vertical axis. The contour levels are at 0.80, 1.00, 1.25, 1.57, 1.96, 2.45, 3.06, 3.83, 4.80, 6.00, and 7.50 mJy Bm^{-1}. From the lower resolution natural weight data.

that there are two peaks at different velocities at that position in panel (b). The integrated H I spectra are shown in Figs. 18 and 19. Both galaxies show typical rotational velocity fields, with the radial velocity of the two galaxies matching smoothly at the bridge. Since the inclination of the galaxies is almost identical, this means that the two galaxies have

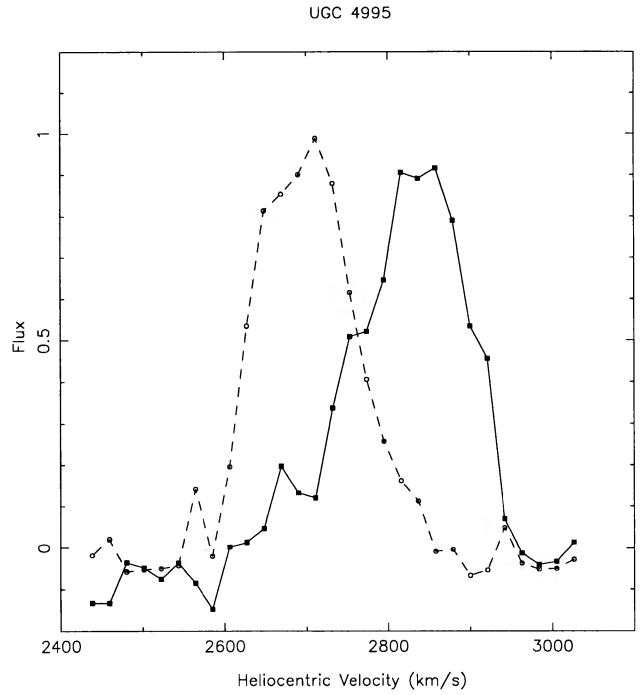

FIG. 7. Integrated H I spectrum for UGC 4995, where the integration excludes the tidal bridge and tail. Made from the lower resolution natural weight data.

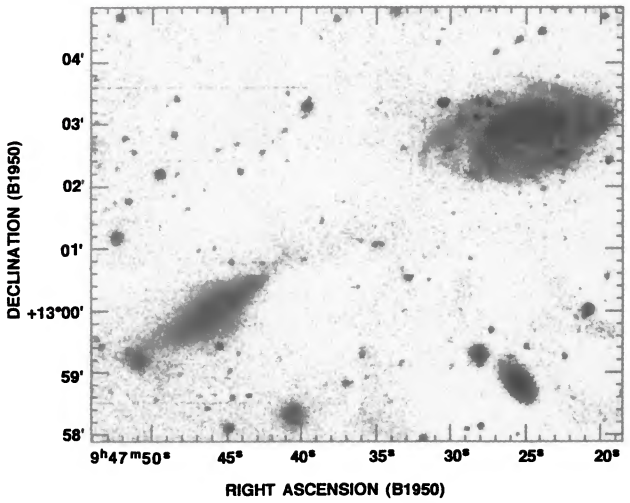

FIG. 8. *R* band image for UGC 5271−5. UGC 5271 is at the upper right and UGC 5275 is at the lower left.

oppositely directed spins. Note that for UGC 9728, the inner contours are almost linearly radial with a slight flattening exactly on the major axis (a comparison with the uniform weight velocity field shows that this flattening is caused by beam smearing). There is also a systematic twisting of the kinematical major axis.

4.5 UGC 9903−4

The *R* band image for UGC 9903−4 is shown in Fig. 20. There is no *V* band image for this pair. The galaxies are

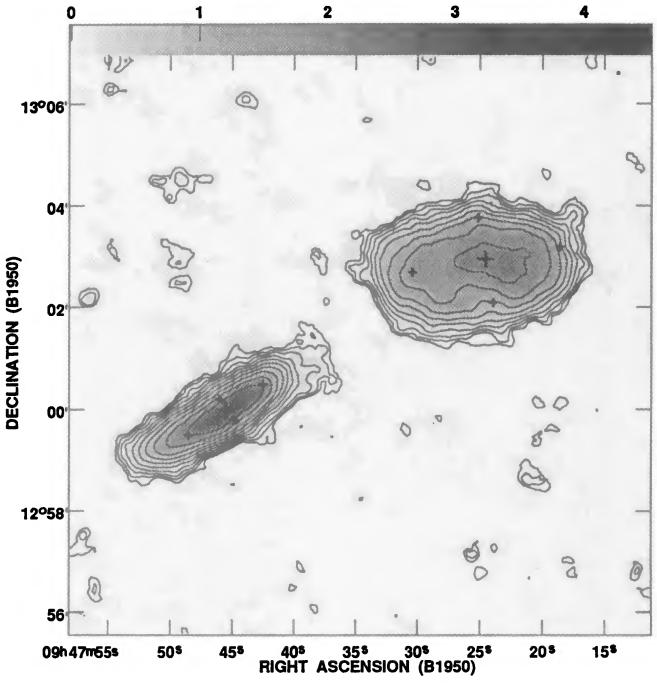

FIG. 9. Contours of constant integrated H I flux for UGC 5271−5, made from the C configuration, natural weight data. The synthesized beam size is 29 arcsec. The contour levels are at 0.12, 0.17, 0.23, 0.33, 0.46, 0.64, 0.89, 1.25, 1.74, 2.43, and 3.40 Jy Bm^{-1} km s^{-1} (~1.6×10^{20} atoms cm^{-2} to ~4.5×10^{21} atoms cm^{-2}). The greyscales range from 0 to 4.5 Jy Bm^{-1} km s^{-1}. The large crosses mark the optical galaxy center, and the smaller crosses mark the tips of the optical major and minor axes.

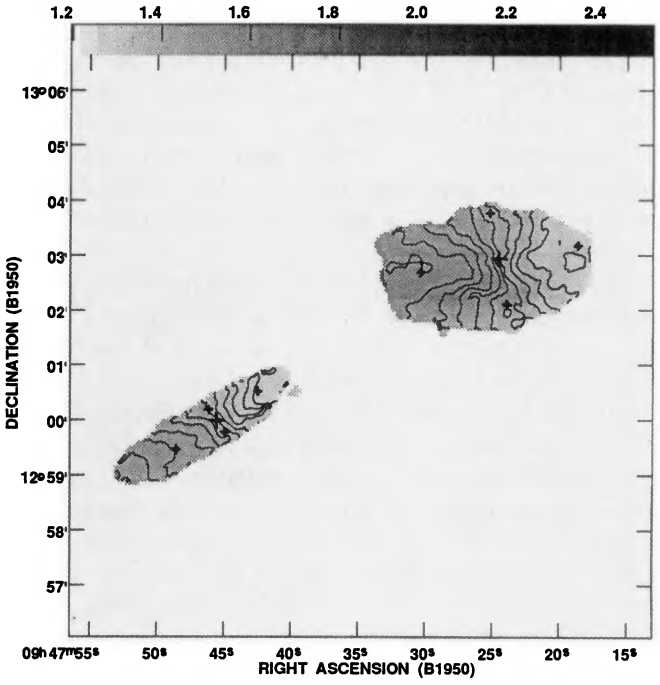

FIG. 10. H I velocity field for UGC 5271−5 (Uniform Weight). There are 17 uniformly spaced contours between 1260 and 1580 km s^{-1} (i.e., 20 km s^{-1} apart). The greyscales range from 1200 to 2500 km s^{-1}. The large crosses mark the optical galaxy center, and the smaller crosses mark the tips of the optical major and minor axes.

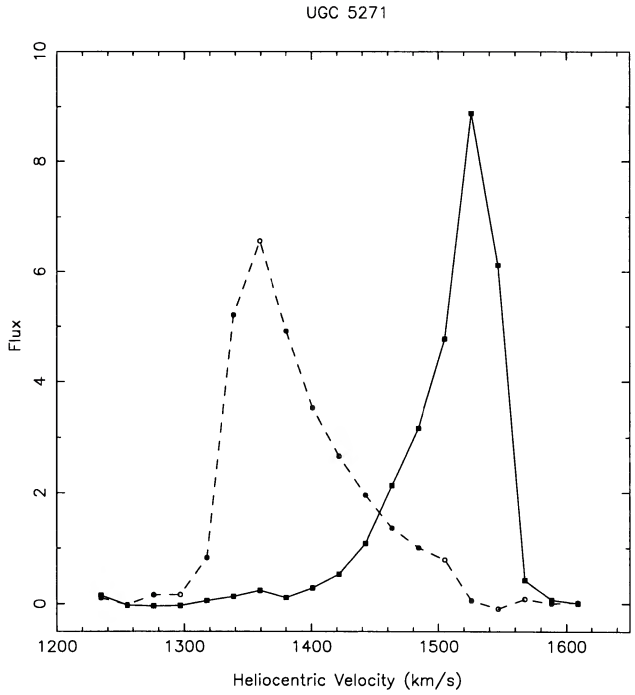

FIG. 12. Integrated H I spectrum for UGC 5271, made from the lower resolution natural weight data.

joined by a broad stellar bridge and the unsharp filtered *R* band image (not included) shows that apart from a central bulge, UGC 9903 is relatively smooth (it has, in fact, been variously classified as an S0 or Sa galaxy), and UGC 9904 has a chain of bright knots running in the north south direction, with the galaxy nucleus at the center of this chain. Two faint, spiral armlike features can also be seen in this galaxy.

The bright object at the south west edge of the disk of UGC 9903 is most definitely a foreground star. The diameter of UGC 9904 as measured from the CCD image is slightly larger than the RC3 Holmberg diameter, however for UGC 9903 the RC3 Holmberg diameter is larger than that measured from the CCD image. It seems likely that the earlier measurements are influenced by confusion due to the foreground star. (Note that since the CCD data were taken under

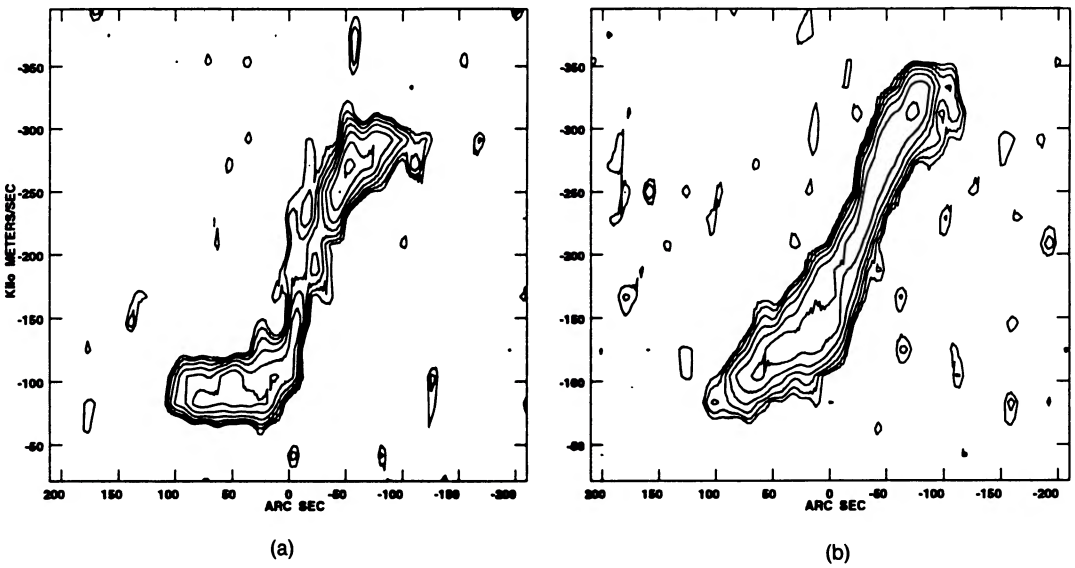

FIG. 11. (a) Contours of constant emission intensity for a cut along the major axis of UGC 5271. The horizontal axis measures distance parallel to the major axis in arcseconds, (the galaxy center is at −23″, east is to the left) velocity (relative to 1630 km s^{-1}) is along the vertical axis. The contour levels are at 1.80, 2.40, 3.19, 4.24, 5.65, 7.51, and 10.00 mJy Bm^{-1}. Made from the high resolution uniform weight data. (b) Contours of constant emission intensity for a cut along the major axis of UGC 5275. The horizontal axes measures distance parallel to the major axes in arcseconds, [the galaxy center is at −25″, east is to the left) velocity (on the same scale as for (a)] is along the vertical axes. The contour levels are at 1.50, 2.23, 3.30, 4.90, 7.27, 10.78, and 16.00 mJy Bm^{-1}. Made from the high resolution uniform weight data.

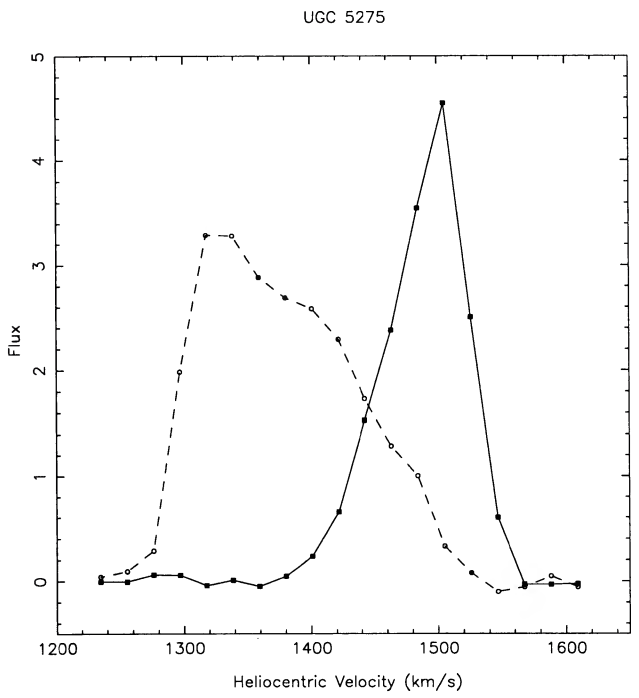

FIG. 13. Integrated H I spectrum for UGC 5275, made from the lower resolution natural weight data.

nonphotometric conditions, the measured diameter does not correspond to a known isophotal level. However, the diameters were measured to the same relative level for both galaxies in the pair).

The integrated H I maps are shown in Fig. 21(a) (natural weight) and Fig. 21(b) (uniform weight), the optical centers and the tips of the major and minor axes are shown by large and small crosses as before. The emission from the two galaxies overlap to a considerable degree, however an extension of the H I distribution along the major axis of UGC 9904 can be clearly seen in both maps.

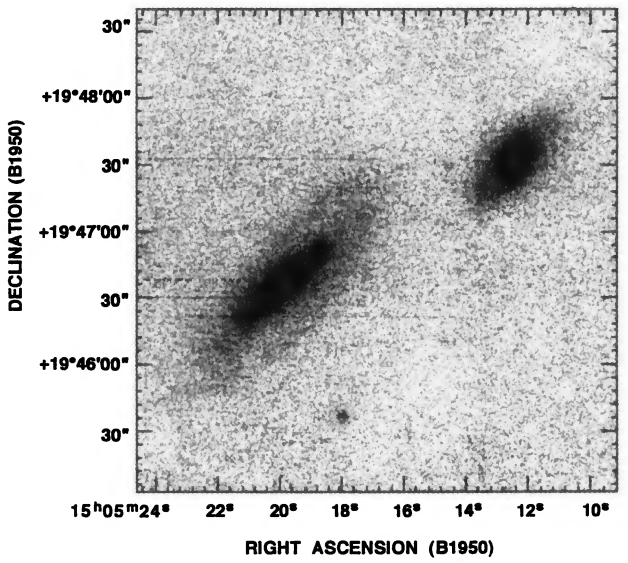

FIG. 14. *R* band image for UGC 9724−8. UGC 9724 is the smaller galaxy on the right and UGC 9728 is the larger galaxy on the left.

The H I distribution at the optical position of UGC 9903 is very asymmetrical, with considerably more H I on the side nearer to UGC 9904 than the side away from UGC 9904. Note that the RC3 Holmberg diameter size (which is probably an overestimate as described above), has been used to mark tips of the major and minor axes. However, the asymmetry persists even if the smaller CCD measured diameters are used.

The most striking feature of the maps however is a plume of hydrogen extending to the north-west. From the inset in Fig. 21(a), (which is a contour plot of the *R* band CCD image, with the foreground star blanked out), it can be seen that the outer isophotes of UGC 9903 show an extension to the north west, at the same position angle as the plume seen in the neutral hydrogen maps. The neutral hydrogen plume of course extends to a much larger galactocentric distance.

In addition to the pair UGC 9903-4, another galaxy, UGC 9902 is detected in the VLA maps. UGC 9902 is a 17th magnitude galaxy, with a UGC classification of SBdm?, and has a correspondingly small velocity width (emission is detected only over a total velocity range of $\sim$120 km s^{-1}, despite the fact that the galaxy is almost edge on).

The velocity field for UGC 9903-4 is shown in Fig. 22 (Natural Weight). The uniform weight map is similar and is not shown. The velocity field is complex, and cannot be easily decomposed. It is curious to note that the velocity contours when combined over the two galaxies give the impression of a single rotating (albeit disturbed) disk, with a kinematic axis running from the south-east to the north-west. As discussed in Sec. *4.1*, velocity fields produced by the moment method tend to be smooth even if there is gas with different velocities along the same line of sight. An examination of the individual channel maps shows that this is not the situation here. In any case, the observed large scale gradient in velocity from the north-west to the south-east could not be an artifact of the moment method. It is also clear that the southern half of UGC 9904 is at a lower heliocentric velocity than the northern half. More tentatively, the south-western half of UGC 9903 is at a higher heliocentric velocity as compared to the north-eastern half. This is difficult to see in the velocity maps because of the overlapping H I distributions in the north-east of UGC 9903, but it is also borne out by examination of the individual channel maps.

Some insight into the H I distribution can be gained by examining the position velocity maps along the optical major axes. For UGC 9904 [Fig. 23 panel (b)], the velocity varies systematically along the major axis, with emission detected from a relative velocity of -100 to -400 km s^{-1}. The position velocity map for UGC 9903 [Fig. 23, panel (a)] is more complicated. For a simple circular rotation with ro tation sense as determined from the the velocity map, the velocity should decrease as one goes from negative to positive displacements along the major axis. This can indeed be seen in Fig. 23 panel (b), but the much stronger feature is at approximately right angles to this, and arises from H I rotating in the same sense as UGC 9904.

The combination of the low inclination of UGC 9903 and the disturbed velocity field of the gas in the galaxy result in a complex integrated spectrum, which is not particularly in-

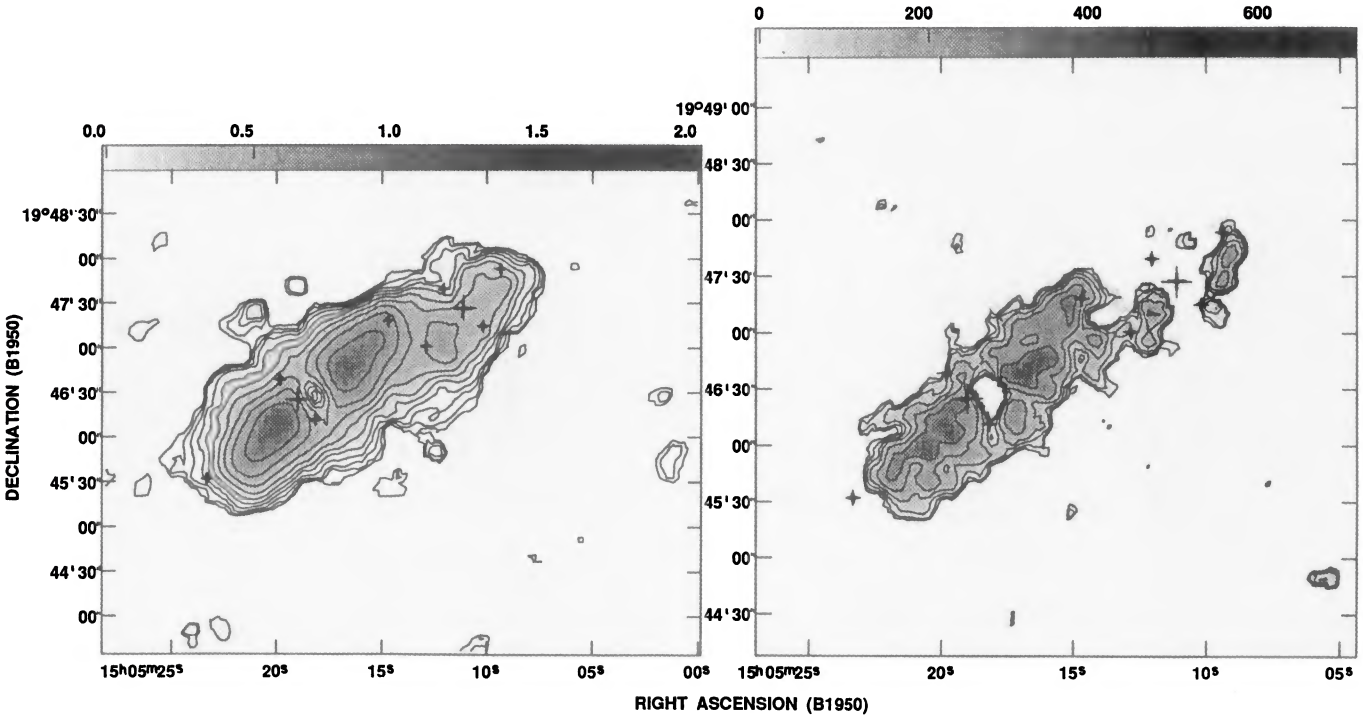

FIG. 15. (a) Contours of constant integrated H I flux for UGC 9724−8, made from the C configuration, natural weight data. The synthesized beam size is 24 arcsec. The contour levels are at 0.03, 0.043, 0.063, 0.091, 0.13, 0.19, 0.27, 0.40, 0.57, 0.82, and 1.19 Jy Bm^{-1} km s^{-1} (~5.8×10^{19} to ~2.3×10^{21} atoms cm^{-2}). The greyscales range from 0 to 2.0 Jy Bm^{-1} km s^{-1}. The large crosses mark the optical galaxy center, and the smaller crosses mark the tips of the optical major and minor axes. (b) Contours of constant integrated H I flux for UGC 9724−8, made from the C configuration, uniform weight data. The synthesized beam size is 12 arcsec. The contour levels are at 0.04, 0.05, 0.08, 0.12, 0.19, 0.28, and 0.43 Jy Bm^{-1} km s^{-1}~2.7×10^{20} to ~3.3×10^{21} atoms cm^{-2}). The greyscales range from 0 to 0.7 Jy Bm^{-1} km s^{-1}. The large crosses mark the optical galaxy center, and the smaller crosses mark the tips of the optical major and minor axes.

formative. However, as can be seen in Fig. 24, the spectrum in the central region (which also corresponds to a peak in the H I emission) is very sharply peaked, and well approximated by a Gaussian. UGC 9904 has a very asymmetric integrated H I spectrum (Fig. 25).

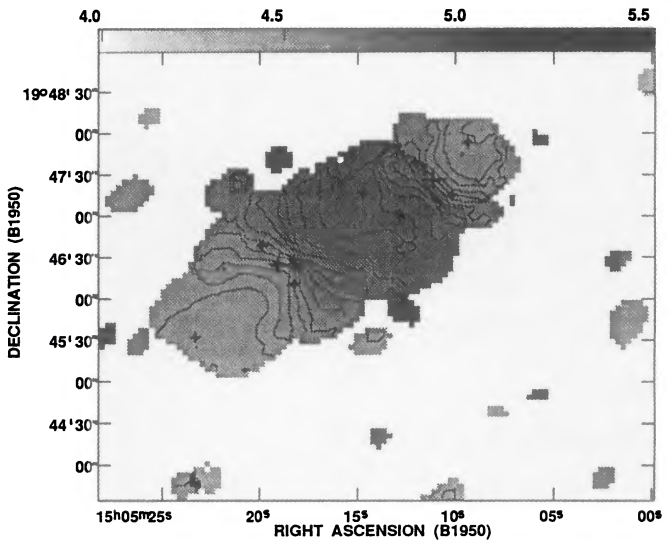

FIG. 16. H I velocity field for UGC 9724−8 (Natural Weight). There are 17 uniformly spaced contours between 4500 and 4980 km s^{-1} (i.e., 30 km s^{-1} apart). The greyscales range from 4000 to 5500 km s^{-1}. The large crosses mark the optical galaxy center, and the smaller crosses mark the tips of the optical major and minor axes.

4.6 UGC 12442−7

The *V* band images for UGC 12442−7 is shown in Fig. 26, the *R* band image is similar and is not shown. Both galaxies are fairly edge on, the *V* band unsharp filtered image (not included) shows that both galaxies are multiarmed spirals, and that UGC 12447 may also possess a central bar. Further, the spiral arms are patchy with several discrete bright knots of emission along the arms.

UGC 12442-7 was observed in both the C and the D configurations of the VLA. As mentioned in Sec. 3, the D configuration maps are affected by solar interference and are not shown. UGC 12442 appears to have a strongly warped H I disk, [Fig. 27(a) (natural weight), and Fig. 27(b) (uniform weight)]. In the natural weight map a warp can be seen clearly at the western end of the disk, while there is a hint of a warp at the eastern end, which can be seen more clearly in the uniform weight map. Note also that the central contours in the uniform weight map are rotated counter-clockwise by about 10 degrees as compared to the natural weight map. Finally, the H I disks of the two galaxies show a much smaller difference in size as compared to the optical disks.

The natural weight map shows that UGC 12447 has an asymmetric H I distribution with the brightest emission displaced towards the companion galaxy. The uniform weight

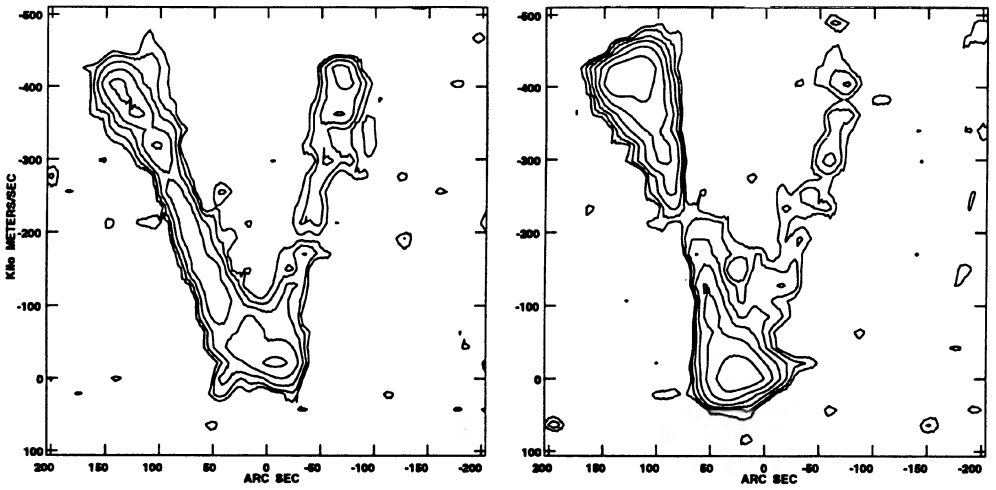

FIG. 17. (a) Contours of constant emission intensity for a cut along the major axis of UGC 9724. The horizontal axis measures distance parallel to the major axis in arcsec (the galaxy center is at −44″, east is to the left), velocity (relative to 4970 km s^{-1}) is along the vertical axis. The contour levels are at 0.7, 1.12, 1.80, 2.90, 4.65, 7.47, and 12.00 mJy Bm^{-1}. Made from the lower resolution, natural weight data. (b) Contours of constant emission intensity for a cut along the major axis of UGC 9728. The horizontal axis measures distance parallel to the major axis in arcseconds (the galaxy center is at 70″, east is to the left), velocity [on the same scale as for (a)] is along the vertical axis. The contour levels are the same as for (a). Made from the lower resolution, natural weight data.

map shows that there is in fact a local minimum in the H I distribution at the center of UGC 12447, with maxima at more or less symmetrically placed on either side of the galaxy center. This is similar to the H I distribution for UGC 9728, and is what is expected from a torus shaped H I distribution.

The position velocity diagrams for the two galaxies (Fig. 29) show asymmetry in the velocity field, particularly UGC 12442 [panel (a)], where the low velocity side shows a rising radial velocity, while the high velocity side shows a falling radial velocity.

The velocity field for UGC 12442−7 is shown in Fig. 28 (uniform weight). For UGC 12442 the receding and approaching sides of the galaxy appear quite different. The receding side has isovelocity contours that close, while the approaching side has open velocity contours. UGC 12447

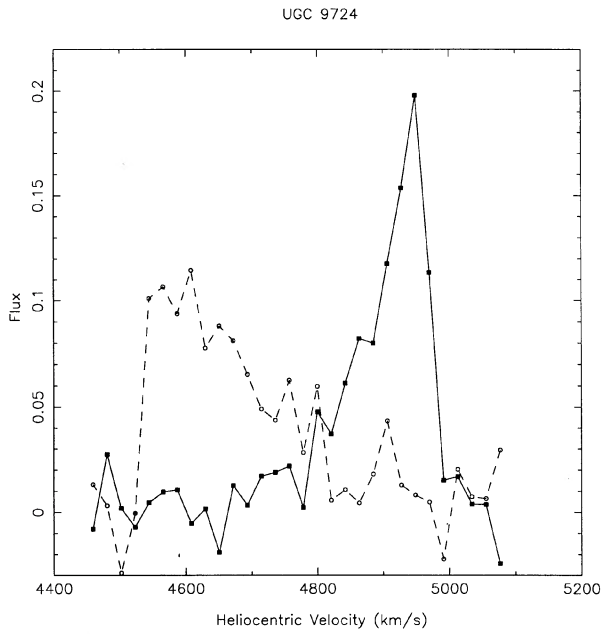

FIG. 18. Integrated H I spectrum for UGC 9724, made from the lower resolution natural weight data.

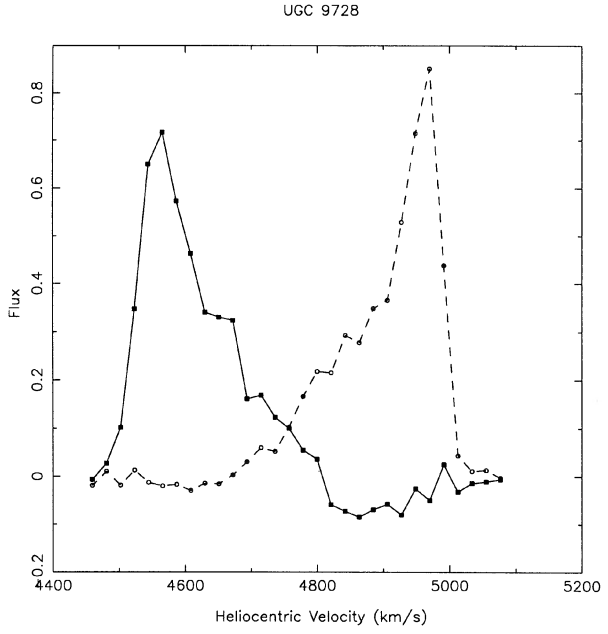

FIG. 19. Integrated H I spectrum for UGC 9728, made from the lower resolution natural weight data.

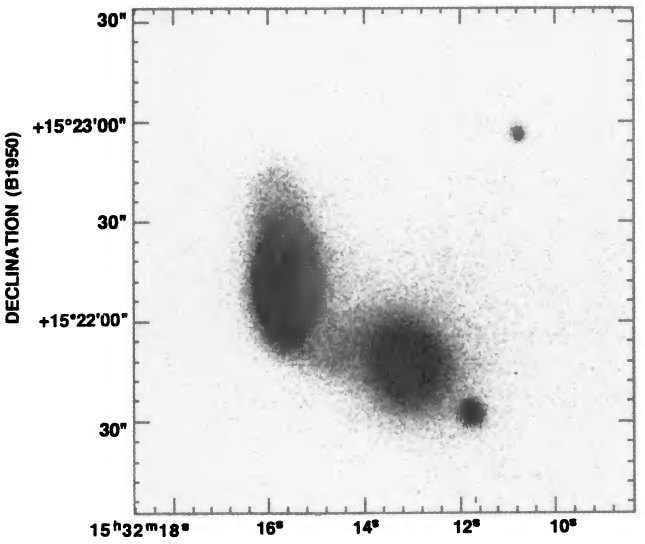

FIG. 20. *R* band image for UGC 9903−4. UGC 9903 is the face on galaxy to the right and UGC 9904 is the edge on galaxy to the left.

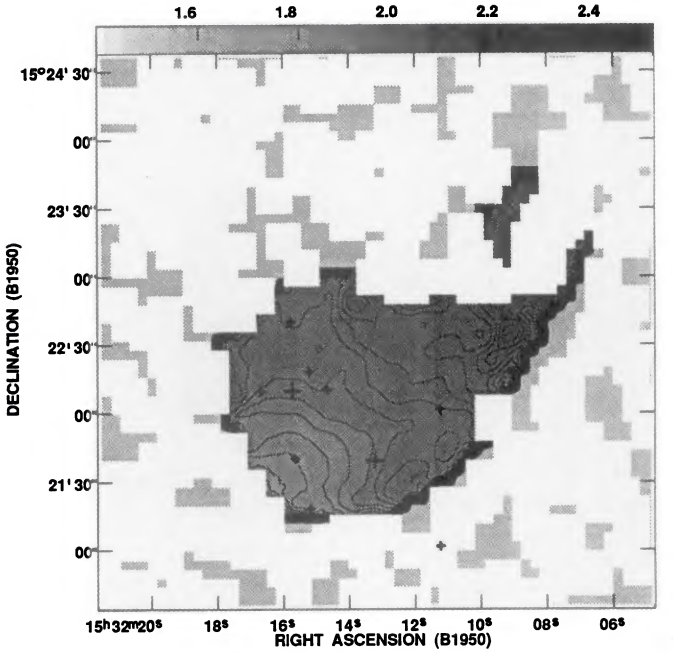

FIG. 22. H I velocity field for UGC 9903−4 (Natural Weight). There are 23 uniformly spaced contours between 1600 and 2150 km s^{-1} (i.e., 25 km s^{-1} apart). The greyscales range from 1400 to 2500 km s^{-1}. The large crosses mark the optical galaxy center, and the smaller crosses mark the tips of the optical major and minor axes.

has a similar asymmetry with closed velocity contours on the receding side. Further, there is also a kink in the velocity contours near the major axis. The integrated H I spectra for the two galaxies are shown in Figs. 30 and 31.

4.6.1 Radio sources around UGC 12442−7

The VLA maps for UGC 12442−7 also show five radio continuum sources more or less symmetrically situated around the galaxy pair [Fig. 32(a)]. The statistical chances of getting these many bright sources to lie by chance near the

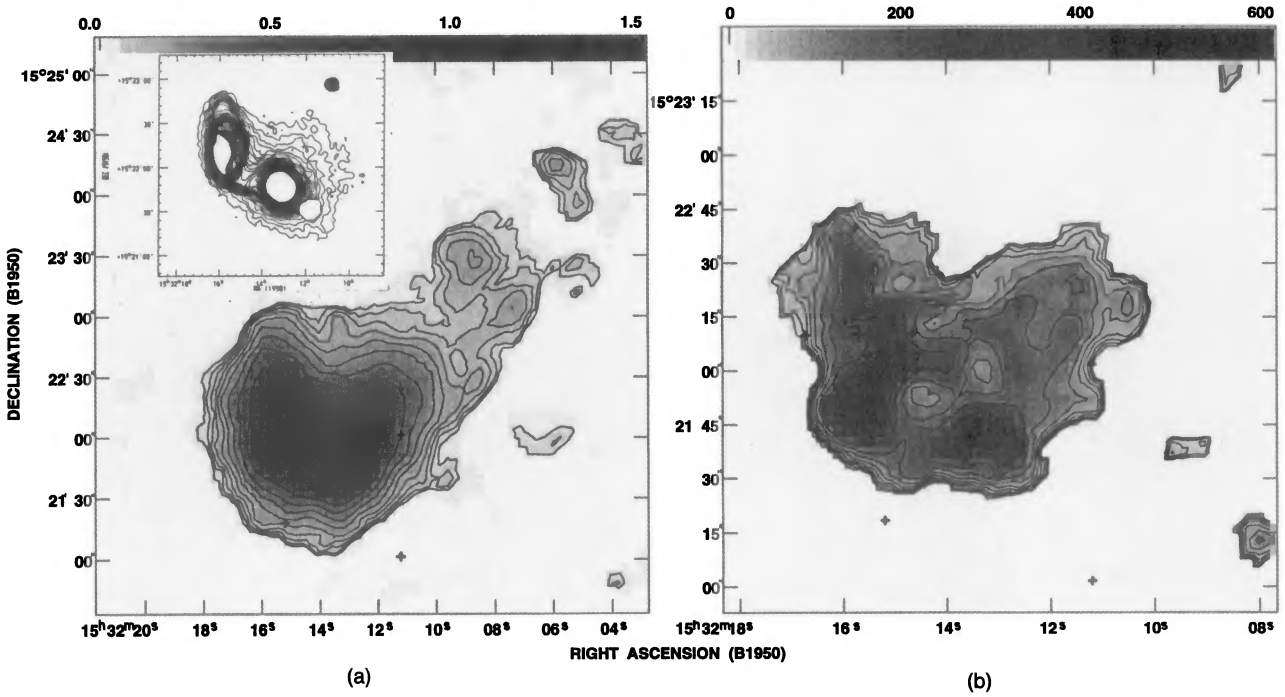

FIG. 21. (a) Contours of constant integrated H I flux for UGC 9903−4, made from the C configuration, natural weight data. The synthesized beam size is 24 arcsec. The contour levels are at 0.05, 0.07, 0.09, 0.12, 0.17, 0.22, 0.30, 0.41, 0.55, 0.74, and 1.00 Jy Bm^{-1} km s^{-1} (~9.6×10^{19} to ~1.9×10^{21} atoms cm^{-2}). The greyscales range from 0 to 1.5 Jy Bm^{-1} km s^{-1}. The large crosses mark the optical galaxy center, and the smaller crosses mark the tips of the optical major and minor axes. (Inset: Isophotal contours for UGC 9903−4 (*R* band). The foreground star to the south-west of UGC 9903 has been blanked out.) (b) Contours of constant integrated H I flux for UGC 9903−4, made from the C configuration, uniform weight data. The synthesized beam size is 12 arcsec. The contour levels are at 0.02, 0.03, 0.04, 0.05, 0.08, 0.10, 0.15, 0.20, 0.28, 0.39, and 0.54 Jy Bm^{-1} km s^{-1} (~1.5×10^{20} to ~4.2×10^{21} atoms cm^{-2}). The greyscales range from 0 to 0.6 Jy Bm^{-1} km s^{-1}. The large crosses mark the optical galaxy center, and the smaller crosses mark the tips of the optical major and minor axis.

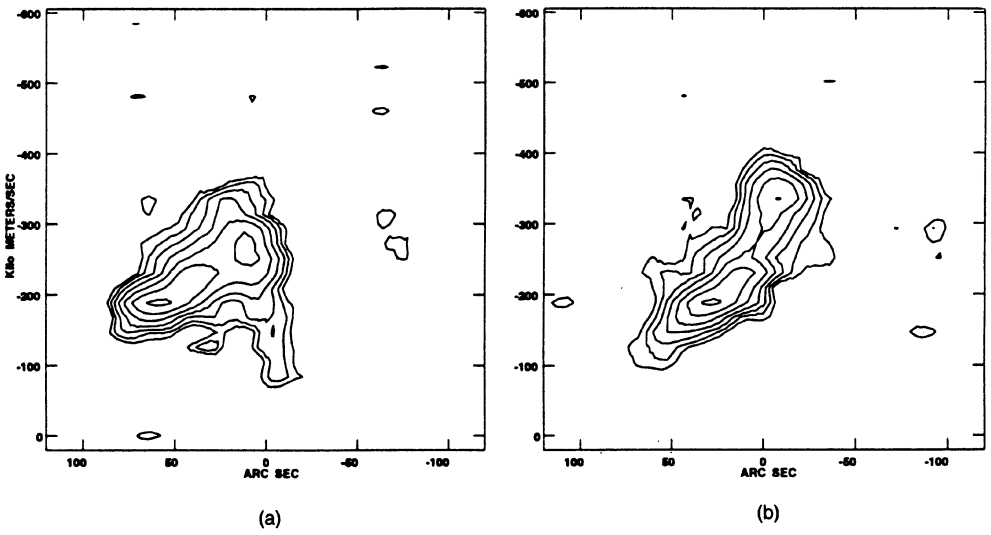

FIG. 23. (a) Contours of constant emission intensity for a cut along the major axis of UGC 9903. The horizontal axis measures distance parallel to the major axis in arcseconds (the galaxy center is at 2″, north-east is to the left), velocity (relative to 2170 km s^{-1}) is along the vertical axis. The contour levels are at 1.20, 1.70, 2.41, 3.41, 4.83, 6.85, and 9.70 mJy Bm^{-1}. Made from the lower resolution natural weight data. (b) Contours of constant emission intensity for a cut along the major axis of UGC 9904. The horizontal axis measures distance parallel to the major axis in arc seconds (the galaxy center is at 15″, north is to the left), velocity [on the same scale as for (a)] is along the vertical axis. Contour levels are as for (a). Made from the lower resolution natural weight data.

galaxy pair are small (see below) but not extremely so. Following the VLA observations, this region of the sky was also mapped at Arecibo at 2380 MHz (i.e., a beam size of ~2.2′). The details of the observational and data reduction procedures can be found in Chengalur (1994). The Arecibo map is shown in Fig. 32(b), and the positions, fluxes and spectral indices of the detected radio sources are listed in Table 3.

The distances to the satellite sources from UGC 12447 vary from 8.1′ to 12.5′, which correspond to linear distances of 83 and 127 kpc at the redshift of the pair. The sources are approximately symmetrically placed around the galaxy pair, and further the minor axis of UGC 12447 lies approximately on the line joining the two strongest sources, C and D. Leaving aside the issue of the symmetry of the arrangement of the sources, what is the probability of observing these many sources in a field picked at random? From the source counts in Condon & Mitchell (1984), the average number of sources with flux greater than 30 mJy in a 16′ diameter region of the

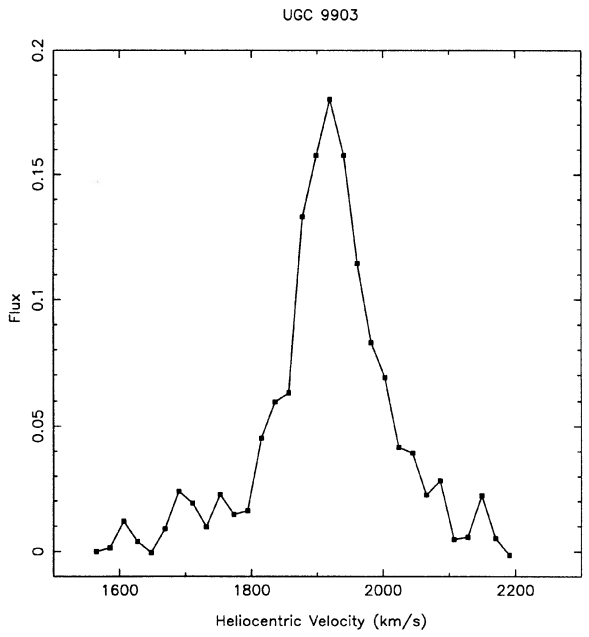

FIG. 24. H I spectrum for the central region (high density peak) UGC 9903, made from the lower resolution natural weight data.

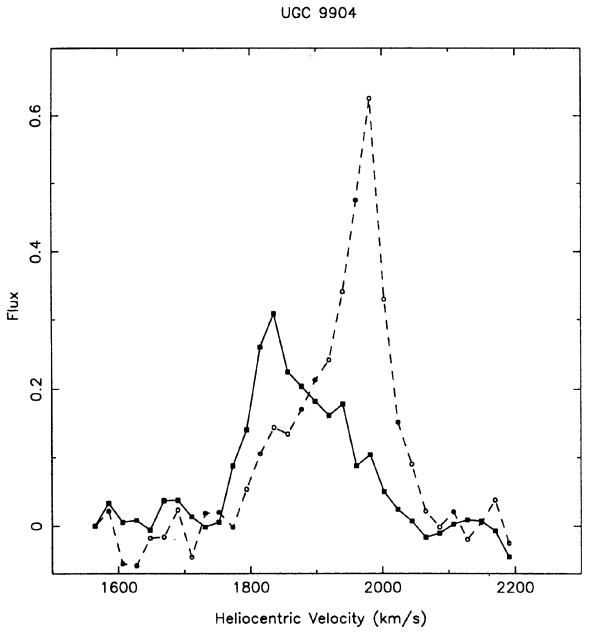

FIG. 25. Integrated H I spectrum for UGC 9904, made from the lower resolution natural weight data.

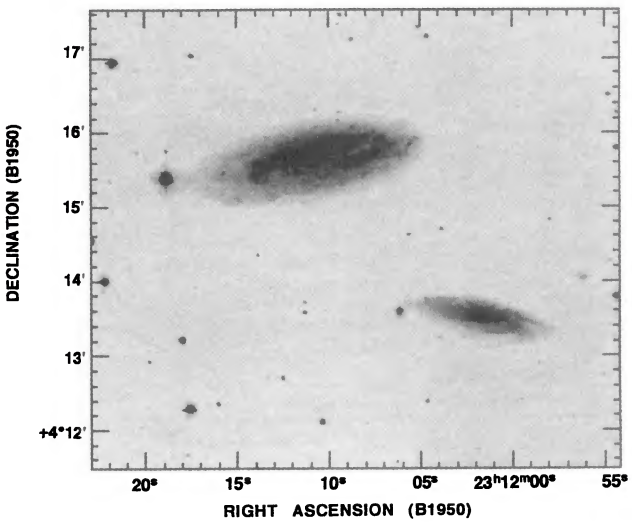

FIG. 26. *V* band image for UGC 12442−7. UGC 12442 is to the lower right and UGC 12447 is to the upper left.

sky (the size of the VLA map) is 1.2. Assuming that radio sources have a Poisson distribution, the probability of obtaining five or more sources is 0.008, or about once every 125 times. Note that this probability was computed using an *a posteriori* selected cutoff level of 30 mJy. These and other related issues are discussed further in Chengalur (1994).

4.7 UGC 12737-8

The *R* band image for UGC 12737-8 is shown in Fig. 33. The *V* band image is similar (except that the galaxies have

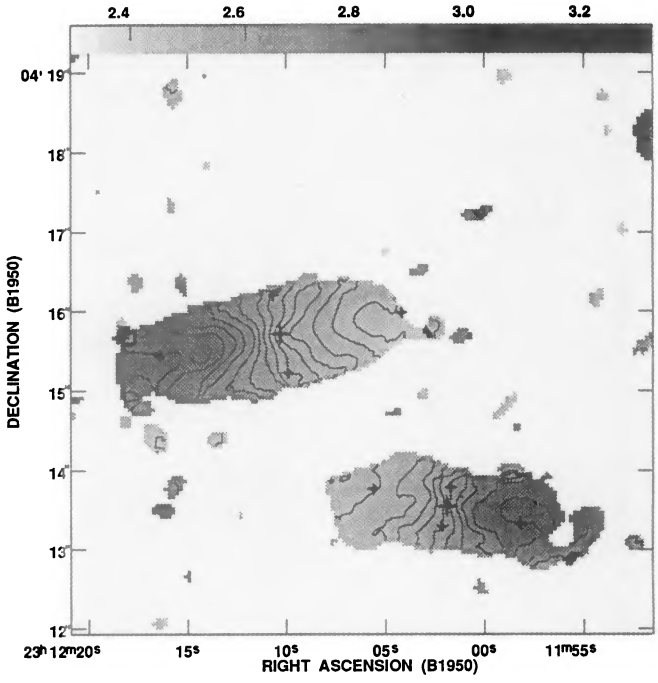

FIG. 28. H I velocity field for UGC 12442−7 (Uniform Weight). There are 21 uniformly spaced contours between 2360 and 2960 km s^{-1} (i.e., 30 km s^{-1} apart). The greyscales range from 2300 to 3300 km s^{-1}. The large crosses mark the optical galaxy center, and the smaller crosses mark the tips of the optical major and minor axes.

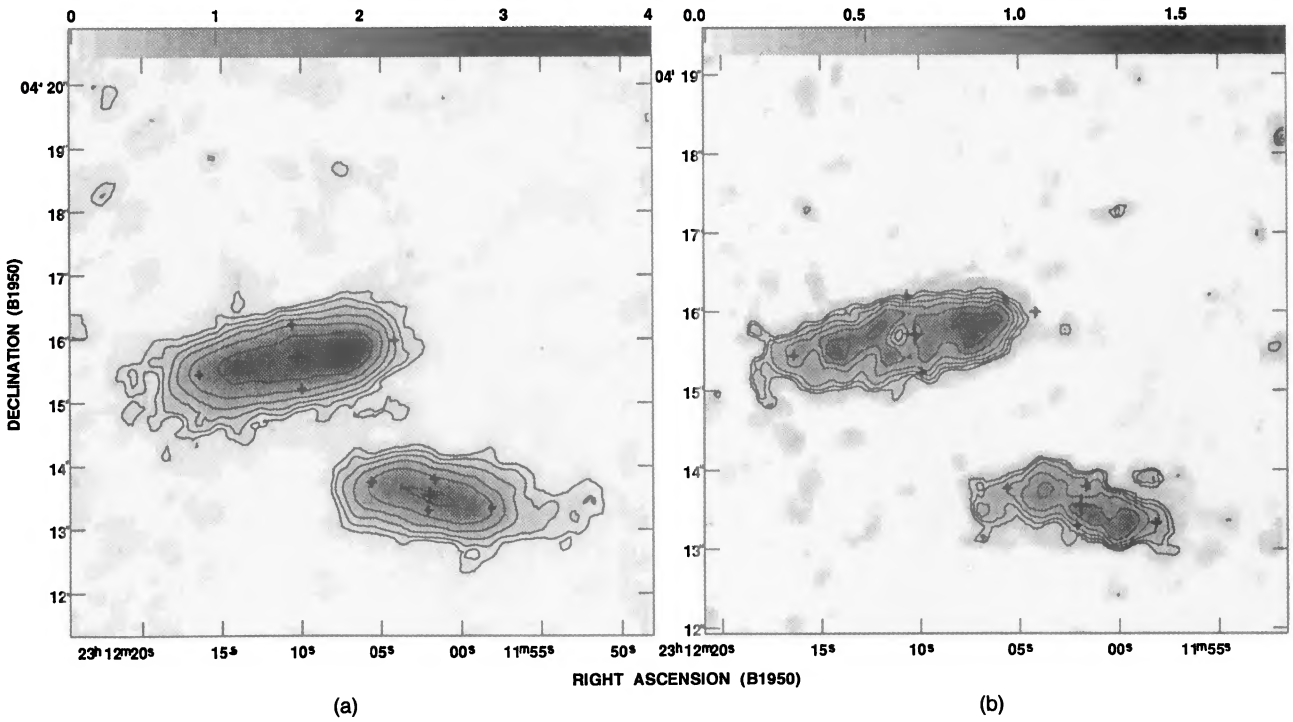

FIG. 27. (a) Contours of constant integrated H I flux for UGC 12442−7, made from the C configuration, natural weight data. The synthesized beam size is 29 arcsec. The contour levels are at 0.20, 0.33, 0.53, 0.86, 1.40, 2.28, and 3.70 Jy Bm^{-1} km s^{-1} (~2.6×10^{20} to ~4.9×10^{21} atoms cm^{-2}). The greyscales range from 0 to 4 Jy Bm^{-1} km s^{-1}. The large crosses mark the optical galaxy center, and the smaller crosses mark the tips of the optical major and minor axes. (b) Contours of constant integrated H I flux for UGC 12442−7, made from the C configuration, uniform weight data. The synthesized beam size is 16 arcsec. The contour levels are 0.25, 0.34, 0.45, 0.61, 0.83, 1.11, and 1.5 Jy Bm^{-1} km s^{-1} (~1.1×10^{20} to ~6.5×10^{21} atoms cm^{-2}). The greyscales range from 0 to 1.8 Jy Bm^{-1} km s^{-1}. The large crosses mark the optical galaxy center, and the smaller crosses mark the tips of the optical major and minor axes.

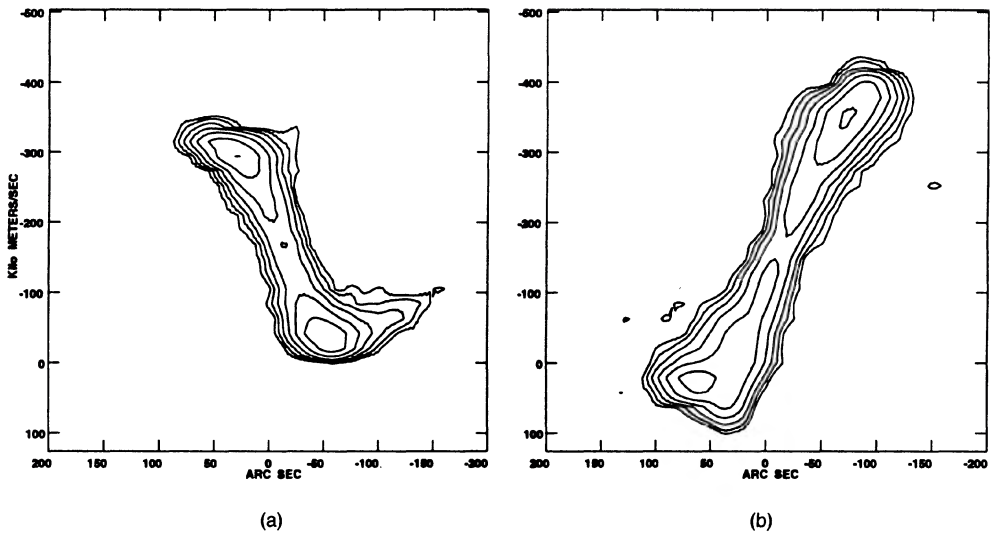

FIG. 29. (a) Contours of constant emission intensity for a cut along the major axis of UGC 12442. The horizontal axis measures distance parallel to the major axis in arcseconds (the galaxy center is at −12″, east is to the left), velocity (relative to 2850 km s^{-1}) is along the vertical axis. The contours are at 2.00, 3.19, 5.10, 8.12, 13.0, 20.7, and 33.0. Made from the lower resolution natural weight data. (b) Contours of constant emission intensity for a cut along the major axis of UGC 12447. The horizontal axis measures distance parallel to the major axis in arcseconds (the galaxy center is at −28″, east is to the left), velocity [on the same scale as for (a)] is along the vertical axis. The contour levels are 2.00, 3.25, 5.29, 8.60, 14.0, 22.8, and 37.0. Made from the lower resolution natural weight data.

been improperly centered on the chip and the eastern tip of UGC 12738 falls on the edge of the image), and is not shown.

UGC 12737 has a diffuse halo, while the central regions are composed of a bar and bulge. The central bar appears to have a different position angle than that of the major axis of the diffuse halo. The ellipticity and position angle of the central bar is 0.35±0.01, 45°±1°. The halo ellipticity and position angle cannot be measured well, but indicative values of 0.2° and 90° could be used.

UGC 12738 shows a very peculiar "dent" at the western end of the disk. The unsharp filtered image (not included) shows that the region of brightest emission bends away from the central plane of the galaxy, and in addition there is emission that runs almost perpendicular to the galaxy disk.

The integrated H I emission maps for this pair are shown

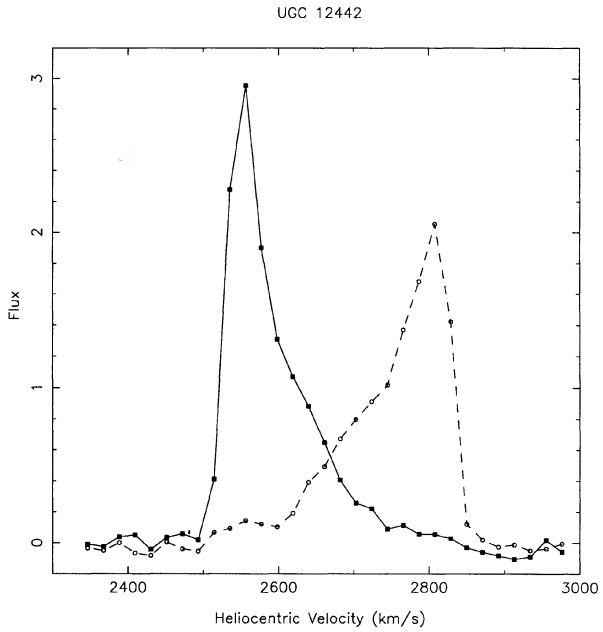

FIG. 30. Integrated H I spectrum for UGC 12442, made from the lower resolution natural weight data.

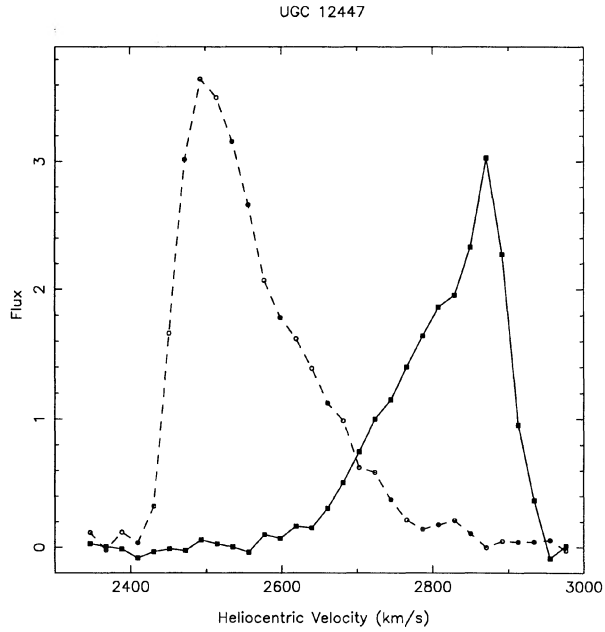

FIG. 31. Integrated H I spectrum for UGC 12447, made from the lower resolution natural weight data.

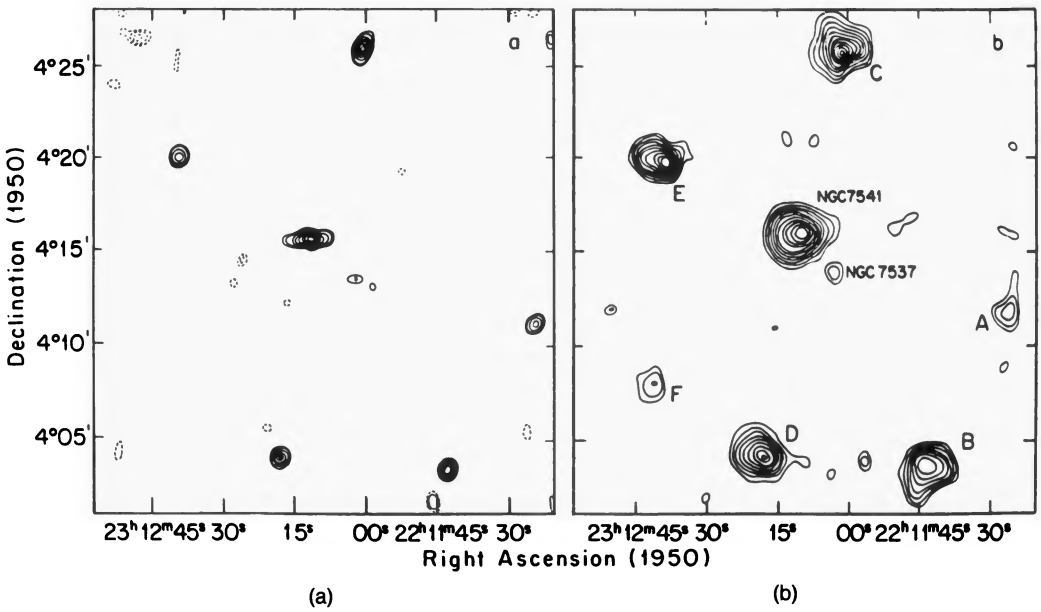

FIG. 32. (a) The VLA 1407 MHz map of the field surrounding the galaxy pair UGC 12442−7 (NGC 7537/7541). The map is produced from the average of all the spectral channels which do not contain line emission. (b) The AO 2380 MHz map of the same field. The radio sources around the pair are labeled from A to F in order of increasing right ascension. The axes scales are identical to those in (a).

in Fig. 34(a) (natural weight) and Fig. 34(b) (uniform weight). Much like UGC 9903−4, the pair has a large common H I envelope, with a clear increase in column density at the position of the edge on galaxy. The H I distribution for UGC 12737 is very smooth, (and is, in fact, largely resolved out in the uniform weight map), with no discernible enhancement in column density towards the central regions.

In the natural weight maps the fainter contours of UGC 12738 can be seen to distort to the south, this is seen even more clearly in the uniform weight map. This is presumably the equivalent to the "dent" in the optical CCD image, although it extends to much larger galactocentric distances.

Again much like UGC 9903−4, the velocity field for common envelope of UGC12737−8 shows a large scale gradient and at first sight gives the impression of being a giant single galaxy in circular (albeit with some disturbances) rotation, (see Fig. 35). However, in this case one can clearly see that there are two kinematic subcenters present,

TABLE 3. Radio sources near UGC 12442−7.

Name	Telescope (VLA/AO)	RA (1950)	Dec (1950)	Flux (mJy)	Spectral Index
U12447	VLA	$23^h\ 12^m\ 11.3^s \pm 0.5^s$	$04^o\ 15'\ 40'' \pm 4''$	152.1	
	AO	231209.7 ± 0.9	041545 ± 12	111.5	−0.6
Src A	VLA	231124.9 ± 0.2	041115 ± 4	32.0	
	AO	231125.2 ± 0.6	041138 ± 11	24.4	−0.6
Src B	VLA	231143.0 ± 0.2	040331 ± 4	48.6	
	AO	231143.3 ± 0.9	040320 ± 13	42.8	−0.2
Src C	VLA	231200.3 ± 0.2	042549 ± 5	118.1	
	AO	231159.7 ± 0.8	042548 ± 11	87.8	−0.6
Src D	VLA	231218.0 ± 0.2	040404 ± 3	67.4	
	AO	231218.6 ± 0.8	040406 ± 10	75.7	0.2
Src E	VLA	231238.8 ± 0.3	042000 ± 5	45.2	
	AO	231238.7 ± 0.9	041954 ± 10	51.2	0.2
Src F	VLA	...	...	...	
	AO	231241.8 ± 0.7	040748 ± 14	19.5	...

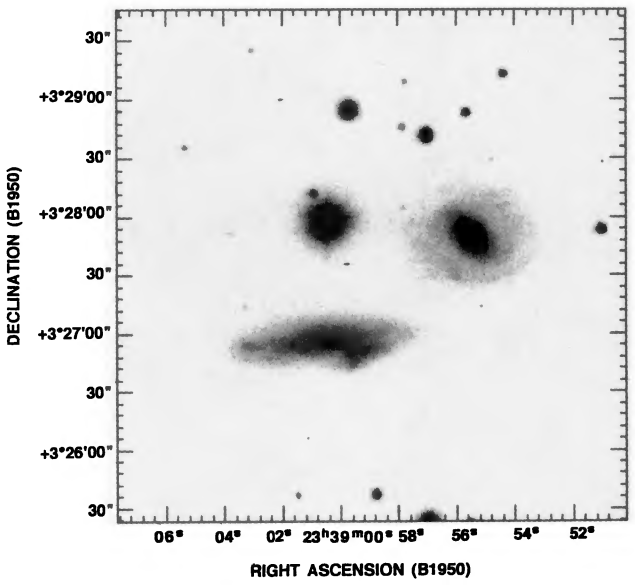

FIG. 33. *R* band image for UGC 12737−8. UGC 12737 is the face on galaxy to the right and UGC 12738 is the edge on galaxy to the left.

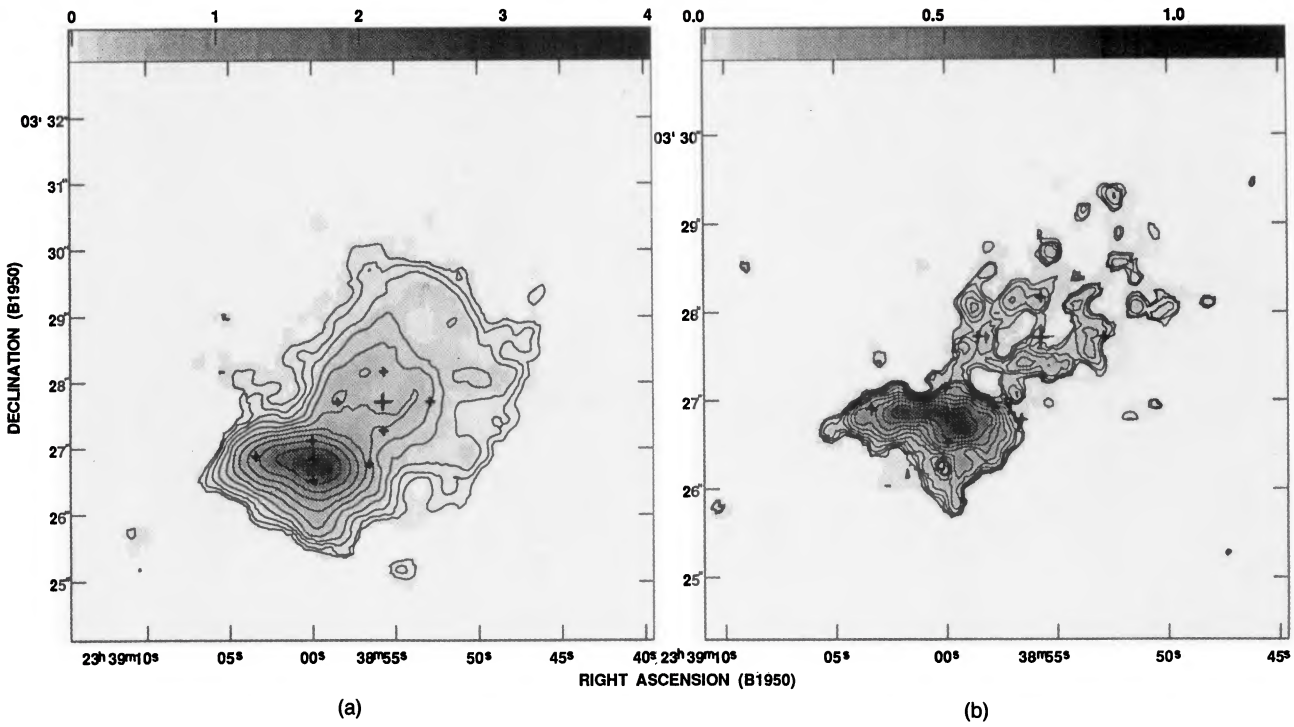

FIG. 34. (a) Contours of constant integrated H I flux for UGC 12737−8, made from the C configuration, natural weight data. The synthesized beam size is 29 arcsec. The contour levels are 0.07, 0.10, 0.14, 0.21, 0.31, 0.46, 0.67, 1.00, 1.47, 2.17, and 3.20 Jy Bm^{-1} km s^{-1} (~8.6×10^{19} to ~4.2×10^{21} atoms cm^{-2}). The greyscales range from 0 to 4.0 Jy Bm^{-1} km s^{-1}. The large crosses mark the optical galaxy center, and the smaller crosses mark the tips of the optical major and minor axes. (b) Contours of constant integrated H I flux for UGC 12737−8, made from the C configuration, uniform weight data. The synthesized beam size is 13 arcsec. The contour levels are at 0.05, 0.07, 0.09, 0.12, 0.16, 0.21, 0.29, 0.38, 0.51, 0.69, and 0.92 Jy Bm^{-1} km s^{-1} (~3.3×10^{20} to ~6.4×10^{21} atoms cm^{-2}). The greyscales range from 0 to 1.2 Jy Bm^{-1} km s^{-1}. The large crosses mark the optical galaxy center, and the smaller crosses mark the tips of the optical major and minor axes.

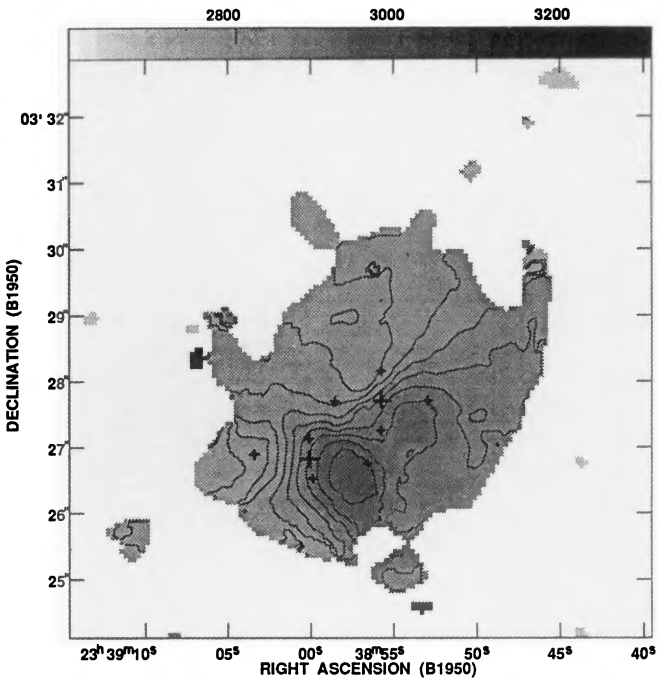

FIG. 35. H I velocity field for UGC 12737−8 (Natural Weight). There are 16 uniformly spaced contours between 2730 and 3030 km s^{-1}, (i.e., 20 km s^{-1} apart). The greyscales range from 2600 km s^{-1} to 3300 km s^{-1}. The large crosses mark the optical galaxy center, and the smaller crosses mark the tips of the optical major and minor axes.

corresponding to the positions of the two galaxies. In the case of UGC 12737 note that in the central region the kinematical major axis is approximately aligned with the central bar seen in the optical CCD images, and not with the major axis of the outer halo.

The position velocity map [Fig. 36, panel (a)] along the central bar of UGC 12737 shows clearly that the radial velocity declines with increasing radius. For UGC 12738, however, [see Fig. 36, panel (b)], the rotation curve appears to be linear over the entire range for which H I emission is seen. There is also a bridge connecting the two galaxies, this can be seen in both panels at a relative velocity of ~−175 km s^{-1}. The integrated H I spectra for the two galaxies are shown in Figs. 37 and 38.

5. SUMMARY AND QUANTITATIVE DATA

As a brief summary of the preceding discussion, morphological features of all the six galaxy pairs are listed in Table 4. The table merely lists whether a given morphological feature is seen in the galaxy or not. In addition to the features listed in Table 4, all the galaxies have disturbed velocity fields, varying from asymmetries between the outer regions of the approaching and receding halves, to sharp kinks in the isovelocity contours in the inner regions of the galaxy, which are probably related to the presence of bars. The various columns of the table are as follows: *Col. (1)*. Galaxy Name (UGC). *Col. (2)*. Does the galaxy have a bar? *Col. (3)*. Are spiral arms detected? *Col. (4)*. Is there a central hole in the

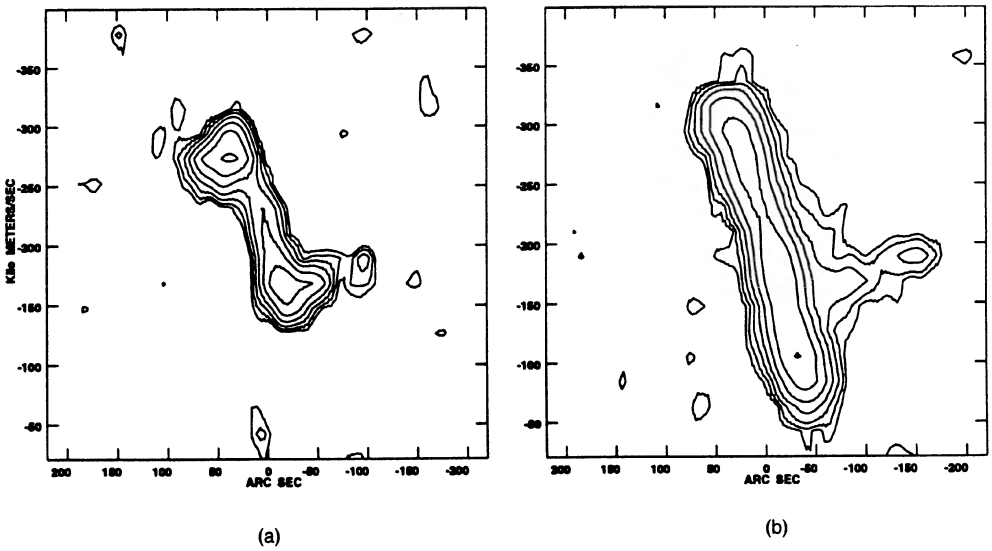

FIG. 36. (a) Contours of constant emission intensity for a cut along the kinematical major axis of UGC 12737. The horizontal axis measures distance parallel to the major axis in arcseconds (the galaxy center is at 5″, north-east is to the left), velocity (relative to 3100 km s^{-1}) is along the vertical axis. The contour levels are at 1.00, 1.41, 2.00, 2.83, 4.00, 5.66, and 8.00 mJy Bm^{-1}. Made from the lower resolution natural weight data. (b) Contours of constant emission intensity for a cut along the major axis of UGC 12738. The horizontal axis measures distance parallel to the major axis in arcseconds (the galaxy center is at −16″, east is to the left), velocity [on the same scale as for (a)] is along the vertical axis. The contour levels are at 1.00, 1.75, 3.07, 5.39, 94.4, 16.6, and 29.0. Made from the lower resolution natural weight data.

H I distribution? *Col. (5)*. Does the pair show tidal tails or bridges? *Col. (6)*. Does the pair have a common H I envelope. Note that for UGC 4995−7, at least part of the common envelope seen in the integrated H I maps is due to beam smearing.

In addition to the qualitative features of the morphology and kinematics, the numerical values of several parameters can be determined from the H I and optical data. From the CCD images the galaxy ellipticity and position angle of the major axis were measured by ellipse fitting done using the task ELLIPSE as embedded in the GALPHOT package of scripts kindly provided by M. P. Haynes. From the average ellipticity, e, of the optical images, the inclination of the galactic disk to the line of sight can be determined. Assuming that the galaxies have an intrinsic axial ratio of r_0=0.2, the inclination angle can be computed from the standard formula,

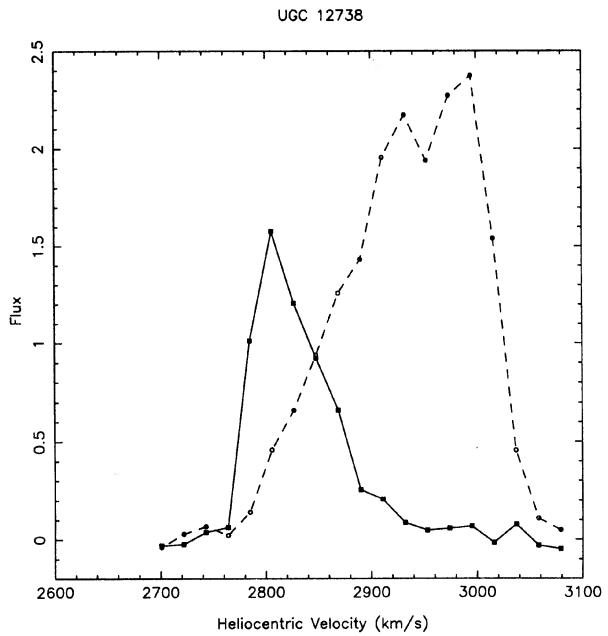

FIG. 37. Integrated H I spectrum for UGC 12737, made from the lower resolution natural weight data.

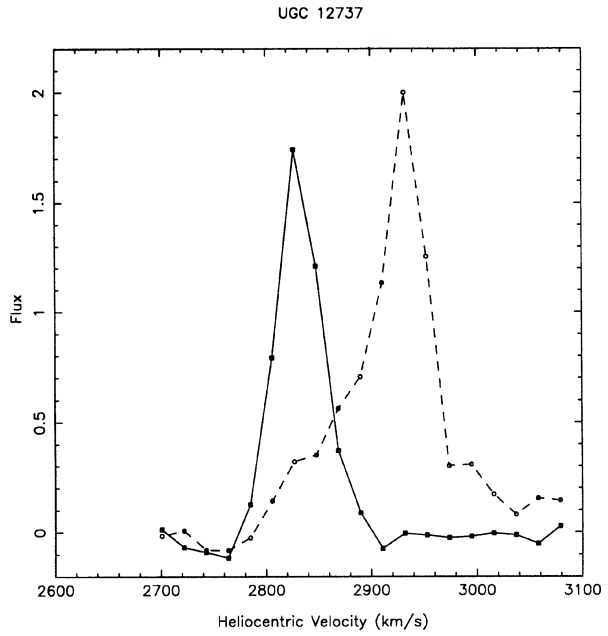

FIG. 38. Integrated H I spectrum for UGC 12738, made from the lower resolution natural weight data.

TABLE 4. Morphology of the close pairs.

Name	Bar	Sp. A.	Hole	Ta/Br	C. E.
U 4995	y	y	n		
U 4997	y	y	n	y	y
U 5271	y	y	n		
U 5275	y	?	n	y	n
U 9724	n	n	y		
U 9728	y	y	y	n	y
U 9903	n	n	n		
U 9904	y	?	n	y	y
U12442	n	y	y		
U12447	?	y	y	n	n
U12737	y	n	n		
U12738	y	?	n	n	y

TABLE 5. Properties of the close pairs.

Name (UGC)	Eps	i (°)	Φ (°)	V_{Helio} (km s^{-1})	V_{max} (km s^{-1})	M_{HI} ($10^9 M_\odot$)
U 4995	0.49 ± 0.05	61 ± 4	235 ± 1	2732 ± 20		2.1
		57 ± 3	227 ± 6	2770 ± 5	305 ± 10	
U 4997	0.56 ± 0.02	66 ± 2	313 ± 2	2638 ± 19		0.3
		...	...	(2714)	(210)	3.3
U 5271	[0.6]	[70]	[100]	1441 ± 1		3.0
		52 ± 2	97 ± 5	1439 ± 5	225 ± 7	
U 5275	0.74 ± 0.02	80 ± 2	124 ± 1	1412 ± 1		1.9
		78 ± 2	125 ± 2	1415 ± 5	240 ± 7	4.9
U 9724	0.47 ± 0.03	60 ± 2	317 ± 1	4772 ± 21		0.9
		...	...	4752 ± 5	439 ± 10	
U 9728	0.67 ± 0.02	75 ± 2	311 ± 1	4764 ± 5		6.8
		...	[135]	4760 ± 5	466 ± 10	7.8
U 9903	0.13 ± 0.01	30 ± 1	217 ± 2	1983 ± 28		0.2
		...	...	(1921)	(200)	
U 9904	0.55 ± 0.04	66 ± 3	2 ± 1	1955 ± 16		0.5
		...	...	1903 ± 5	217 ± 10	1.3
U12442	0.69 ± 0.02	76 ± 2	257 ± 1	2648 ± 28		5.0
		...	[260]	2683 ± 4	308 ± 7	
U12447	0.69 ± 0.03	76 ± 3	100 ± 1	2678 ± 7		9.3
		...	[100]	2681 ± 4	449 ± 7	14.3
U12737	[0.2]	[40]	[27]	2891 ± 7		1.1
		...	...	2885 ± 4	156 ± 10	
U12738	0.71 ± 0.02	77 ± 3	266 ± 2	2907 ± 2		4.3
		[75]	[270]	2904 ± 5	247 ± 10	7.2

$$\cos^2 i = \frac{r^2 - r_0^2}{1 - r_0^2},$$

where $r = 1 - e$ is the axial ratio of the galaxy.[1]

By model fitting to the H I velocity field, (i.e., the "tilted rings" model, see, for example, Begeman 1987), the galaxy's kinematical inclination angle, systemic radial velocity, maximum rotational velocity, and kinematical position angle can be measured. Once again, for sophisticated mass model derivation from rotation curves it may be preferable to use the Gaussian decomposition method to derive the velocity field. However, since we are mainly interested in the global parameters, the MOMNT method is more than adequate. For galaxies with sufficiently regular velocity fields, the iterative fit to the galaxy velocity fields was done using the AIPS task "GAL." Finally, from the integrated H I spectra presented in Sec. 4, the galaxy systemic velocity and the width of the H I profile can be measured.

The columns of Table 5 are as follows. *Col. (1)*. UGC name of the galaxy. *Col. (2)*. Average ellipticity computed from ellipse fits to the CCD image. *Col. (3) Row (1)*. Inclination angle (in degrees) computed from the ellipticity listed in col. (2). Note that the inclination angle is defined to lie between 0° and 90°. *Row (2)*. Inclination angle as derived from the H I velocity field. *Col. (4) Row (1)*. Average position angle (in degrees) of the major axis computed from ellipse fits to the CCD image. The position angle refers to the receding half of the major axis and is measured eastward of north. *Row (2)*. Position angle of the receding half of the major axis as derived from the H I velocity field. *Col. (5) Row (1)*. The heliocentric velocity and velocity error (in km s^{-1}) for the galaxy. For all cases except UGC 5271 and UGC 5275 the velocity is from the CfA catalog. UGC 5271−5 has an angular separation larger than the Arecibo beam and consequently has good H I measurements. *Row (2)*. The heliocentric velocity as measured from the integrated H I spectrum. In those cases for which the velocity field was regular enough for an iterative fit, the derived systemic velocity agrees with the tabulated velocity to within the errors. *Col. (6)*. The 50% width of the integrated H I profile. Note that no correction has been applied for the galaxy inclination angle. *Col. (7) Row (1)*. The H I mass of the galaxy, in units of $10^9 \mathcal{M}_\odot$. The mass listed in this column refers to the emission that can be readily associated with the galaxy. *Row. (2)*. The total H I mass detected, in units of $10^9 \mathcal{M}_\odot$. This includes emission from both pairs, and any bridges or other peculiar structures.

[1]The ellipticity is defined to be $e = 1 - b/a$, where a and b are the major and minor axes, respectively, of an elliptical contour.

6. CONCLUSIONS

Broadband optical and H I integrated emission and kinematical data were presented for a sample of six binary galaxies. The sample was chosen from the CfA redshift survey using objective selection criteria which were completely independent of any previously known morphological peculiarities. Nonetheless, all the galaxy pairs show morphological and/or kinematical disturbances, verifying that the selection criteria had in fact been quite well tailored to select physically associated galaxy pairs.

Detected tidal features include prominent tails and bridges, as well as common H I envelopes surrounding both galaxies in the pair. The common H I envelope shows a large scale velocity gradient, and appears to be in rotation about a single kinematical axis.

There is relatively good agreement between the optical and H I images, with similar features being seen in both. However, the H I features typically extended to much larger galactocentric distances than the corresponding optical features. In at least one galaxy (UGC 4997), the stellar disk

appears relatively undisturbed while the H I disk is disturbed even towards the central parts of the galaxy.

The systemic velocity difference for the galaxy pairs has been measured quite accurately either from the integrated H I spectral profile, or from a global fit to the galaxy velocity fields. The median velocity difference for the six galaxy pairs is very small, $\sim$20 km s^{-1}. Detailed analysis of the data will be presented in a separate paper.

We are grateful to M. Goss for providing test time at the VLA and for many useful comments. E. Brinks, C. Taylor, P. Perley, and D. Wonker provided considerable help with the VLA observations and data reduction while J. Carrasco, J. Henning, D. Tennant, and R. Thicksten provided help and advice with the Palomar observations. Helpful discussions with S. Schneider, J. Charlton, M. P. Haynes, R. Giovanelli, S. Gelato, and especially, A. Broeils are also gratefully acknowledged. We would like to thank J. Huchra for providing a computer readable version of the CfA catalog. This work was supported in part by the National Astronomy and Ionosphere Center, which is operated by Cornell University under a cooperative agreement with the National Science Foundation, and in part by NSF Grant No. AST 91-19475.

REFERENCES

Begeman K. 1987. Ph.D thesis, Groningen University
Charlton, J., & Salpeter, E. E. 1991, ApJ, 375, 517
Chengalur, J. N., Salpeter, E. E., & Terzian Y. 1993, ApJ, 419, 30
Chengalur, J. N. 1994, Ph.D. thesis, Cornell University
Chengalur, J. N., Salpeter, E. E., & Terzian, Y. 1994, in preparation
Condon, J. J., & Mitchell, K. J. 1984, AJ, 89, 610
de Vaucouleurs, G., de Vaucouleurs, A., Corwin, H. G., Buta, R. J., Paturel, G., & Fouque, P. 1992, Third Reference Catalogue of Bright Galaxies (Springer, Berlin)
Haynes, M. P., & Giovanelli, R. 1992, private communication
Howard, S., Keel, W. C., Byrd, G., & Burkey, J. 1993, ApJ (in press)
Huchra, J. P., Davis, M., Latham, D. W., & Tonry, J. 1983, ApJS, 52, 89
Karachentsev, I. D. 1972, Comm. Spec. Ap. Obs. U.S.S.R, 7, 1
Megeath, S. T. 1993, Ph.D. thesis, Cornell University
Miller, R. H., & Smith, B. F. 1979, ApJ, 227, 785
Page, T. 1952, ApJ, 116, 63
Peterson, S. D. 1979, ApJ, 232, 20
Schneider, S. E., & Salpeter, E. E. 1992, ApJ, 385, 32
Schweizer, Y. L. 1987, ApJS, 64, 427
Sharp, N. A. 1990, ApJ, 354, 418
Soares, D. S. L. 1990, A&A, 232, 50
Thomasson, M. D., *et al.* 1989, A&A, 211, 25
Turner, E. L. 1976, ApJ, 208, 20
Turner, E. L. 1979, ApJ, 231, 645
van Moorsel, 1992. Ph.D. thesis, University of Groningen
White, S. D. M. 1981, MNRAS, 189, 831
White, S. D. M. Huchra, J., Latham, D., & Davis, M. 1983, MNRAS, 203, 701